

## An improved GRACE monthly gravity field solution by modelling the non-conservative acceleration and attitude observation errors

Qiuji Chen<sup>1,2,3</sup>, Yunzhong Shen<sup>1</sup>, Wu Chen<sup>2</sup>, Xingfu Zhang<sup>4</sup>, Houze Hsu<sup>5</sup>

1. College of Surveying and Geo-Informatics, Tongji University, Shanghai, China
2. Department of Land Surveying and Geo-Informatics, Hong Kong Polytechnic University, Hong Kong
3. Center for Spatial Information Science and Sustainable Development, Shanghai, China
4. Departments of Surveying and Mapping, Guangdong University of Technology, Guangzhou, China
5. State Key Laboratory of Geodesy and Earth's Dynamics, Institute of Geodesy and Geophysics, CAS, Wuhan, China

**Abstract:** The main contribution of this study is to improve the GRACE gravity field solution by taking errors of non-conservative acceleration and attitude observations into account. Unlike previous studies, the errors of the attitude and non-conservative acceleration data, and gravity field parameters, as well as accelerometer biases are estimated by means of weighted least squares adjustment. Then we compute a new time series of monthly gravity field models complete to degree and order 60 covering the period Jan. 2003 to Dec. 2012 from the twin GRACE satellites' data. The derived GRACE solution (called Tongji-GRACE02) is compared in terms of geoid degree variances and temporal mass changes with the other GRACE solutions, namely CSR RL05, GFZ RL05a, and JPL RL05. The results show that (1) the global mass signals of Tongji-GRACE02 are generally consistent with those of CSR RL05, GFZ RL05a, and JPL RL05; (2) compared to CSR RL05, the noise of Tongji-GRACE02 is reduced by about 21% over ocean when only using 300 km Gaussian smoothing, and 60% or more over deserts (Australia, Kalahari, Karakum and Thar) without using Gaussian smoothing and decorrelation filtering; and (3) for all examples, the noise reductions are more significant than signal reductions, no matter whether smoothing and filtering are applied or not. The comparison with GLDAS data supports that the signals of Tongji-GRACE02 over St. Lawrence River basin are close to those from CSR RL05, GFZ RL05a and JPL RL05, while the GLDAS result shows the best agreement with the Tongji-GRACE02 result.

**Keywords:** Satellite geodesy; GRACE; Monthly gravity field model; Non-conservative acceleration

### 1. Introduction

It has almost been 13 years since the Gravity Recovery and Climate Experiment (GRACE) mission was launched to observe temporal variations of the Earth's gravity field. The data collected by the GRACE mission, including the orbits, ranges, attitudes and non-conservative accelerations, allow scientists to determine time-variable gravity with a spatial resolution of about 400 km and a

temporal resolution of one month (Tapley et al. 2004a, 2004b). The mass changes in atmosphere, ocean and land can be effectively detected by using the time-variable gravity field solutions (Tapley et al. 2004b; Chen et al. 2007). Currently, the main monthly gravity field solutions available on the website of International Centre for Global Earth Models (<http://icgem.gfz-potsdam.de/ICGEM/>), are CSR RL05 (Bettadpur 2012), GFZ RL05a (Dahle et al. 2012), JPL RL05 (Watkins et al. 2012), CNES/GRGS (Bruinsma et al. 2014), Tongji-GRACE01 (Chen et al. 2015a), ITG-GRACE2010 (Mayer-Gürr et al. 2010), ITSG-Grace2014 (Mayer-Gürr et al. 2014), and DMT-1 (Liu 2008), as well as AIUB (Meyer et al. 2012). All of these solutions are contaminated by the well-known north-south stripes. To reduce the north-south stripes of the GRACE solutions, a common way is to use decorrelation techniques, such as the  $P_4M_6$  decorrelation filtering (Chen et al. 2009a). The others such as mascon solutions from JPL (Watkins et al. 2015), NASA GSFC (Luthcke et al. 2013) and adaptive filter (Loomis and Luthcke 2014) can greatly improve the GRACE solutions. However constraint or dynamical equations are needed in these solutions. The fact is that the decorrelation filtering not only reduces the noise, but it also weakens the real signals (especially in those areas with small amplitude of signals). Thus, reducing the effects of error sources, for examples, the observation errors of the non-conservative accelerations and attitudes is crucial for the further improvement on the GRACE solutions.

In the determination of these monthly solutions, conservative forces acting on the twin satellites are modelled by background force models, while the non-conservative forces are removed by using the observations of the GRACE onboard accelerometers. **To a great extent the quality of the gravity field solution depends on the onboard accelerometers' performances**, since the twin satellites are flying at a low altitude of around 500 km (Schmidt et al. 2006). In most approaches for achieving these monthly solutions, such as dynamic approach (Bettadpur et al. 2012; Dahle et al. 2012; Watkins et al. 2012), short arc approach (Mayer-Gürr 2006), and modified short arc approach (Shen et al. 2013; Chen et al. 2015a; 2015b; 2015c), the non-conservative acceleration and attitude observations are required to be continuous in order to compute reference orbits based on numerical integration. Due to data gaps of the non-conservative acceleration and attitude observations (especially the data gaps for attitude occur frequently), **some interpolation methods are used for calculating those values at intermediate epochs** (Wu et al. 2006). In the data processing for these monthly gravity field solutions, the non-conservative accelerations and attitudes were treated as error-free observations.

**The non-conservative acceleration observations of the twin satellites are gathered by SuperSTAR accelerometer sensors, and the attitude measurements are collected by star camera sensors. Each SuperSTAR accelerometer sensor has two sensitive axes (namely along track and radial axes)**

and one less sensitive axis (typically cross track axis). The nominal accuracies of the accelerometer sensors are  $10^{-10}\text{m/s}^2$  for the sensitive axes and  $10^{-9}\text{m/s}^2$  for the less sensitive one (Flury et al. 2008). One boresight axis (typically Z axis) and two cross-boresight axes (typically X and Y axes) are possessed by each star camera sensor. The star camera sensor shows much more sensitivities to rotations about the cross-boresight axes than that about the boresight one (Bandikova and Flury 2014; Inacio et al. 2015). Measurements collected by the star camera sensor have a claimed accuracy of  $240\text{ }\mu\text{rad}$  for the rotations about both cross-boresight axes and  $30\text{ }\mu\text{rad}$  for the rotation about the boresight one (Stanton 2000). The rotation matrix from the inertial system to the Science Reference Frame (SRF) is provided by JPL in terms of quaternion elements. Due to the limited sensitivities of these sensors, the attitude and non-conservative acceleration measurements certainly contain observation errors. The imperfect interpolation methods also lead to additional errors for those intermediate epochs. Therefore treating the attitude and non-conservative acceleration data as error-free measurements will certainly affect the estimated gravity field solution.

Although the previous studies (e.g. Horwath et al. 2011; Bandikova et al. 2012; Bandikova and Flury 2014; Klinger et al. 2014; Inácio et al. 2015) discussed the impacts of the attitude errors on the gravity field solutions, the attitude errors are not yet estimated in the gravity field determinations. In principle, the accelerometer data with outliers should be removed or down weighted in the gravity field recovery, while the existing studies concerning the quality of the non-conservative acceleration observations are very limited. A direct way to assess the quality of the accelerometer data is to investigate the non-conservative acceleration noise at high frequencies (Frommknecht 2007; Flury et al. 2008). Mayer-Gürr et al. (2007) derived a static gravity field model called ITG-Grace02s using range measurements by considering the errors of accelerometer data; however the errors of attitude observations were still ignored. Tongji-GRACE01 monthly solutions were developed using the modified short approach (Chen et al. 2015a), which solves the geopotential coefficients and the accelerometer biases by only considering the errors of the satellite orbits and K-band range-rate measurements. Similar to the other existing monthly solutions, neither the attitude errors nor the non-conservative acceleration errors were taken into account in deriving Tongji-GRACE01. To our knowledge, nearly no investigation has so far estimated the unknown geopotential spherical harmonic coefficients together with the errors of the attitude and non-conservative acceleration measurements. These errors will of course, **more or less contaminate the recovered gravity field**. Therefore, in this study, functional models to estimate the errors of the non-conservative acceleration and attitude observations are established, in which the errors of the attitude and non-conservative acceleration data, and the unknowns of the gravity field, as well as the accelerometer biases are

simultaneously estimated by using a weighted least squares adjustment. With this approach, a new time series of GRACE monthly solutions entitled Tongji-GRACE02 complete to degree and order 60 for the period Jan. 2003 to Dec. 2012, is presented in this paper. This paper is organized as follows: in Section 2, the methodology for modelling the errors of the non-conservative acceleration and attitude data on the basis of the modified short arc approach (Chen et al. 2015a) is given. In Section 3, the effects of the modelling of the non-conservative acceleration and attitude measurement errors and data processing procedures for deriving our monthly solutions are discussed. In Section 4, the improvement of Tongji-GRACE02 monthly solutions over ocean is discussed. Section 5 analyzes the performance of Tongji-GRACE02 monthly solutions **compared to some other solutions**. The comparison with GLDAS data is given in Section 6. Section 7 is for the conclusions.

## 2. Mathematical Model

### 2.1 Short arc approach

The short arc integration approach was first presented by Schneider (1968) for satellite orbit determination, then was developed by Mayer-Gürr (2006) for gravity field determination, in which orbit corrections should be computed beforehand. Other short arc techniques such as that proposed by Rowlands et al. (2002) can also be used for the gravity field determination. Recently, a modified short arc approach was proposed in Shen et al. (2013) and Chen et al. (2015a), which simultaneously estimated the orbit corrections and gravity field parameters. In the modified short arc approach, the linearized observation equations for position and velocity vectors can be summarized as,

$$\mathbf{r}(\tau_i) + \mathbf{v}_r(\tau_i) = (\mathbf{r}_0 + \mathbf{v}_{r_0})(1 - \tau_i) + (\mathbf{r}_N + \mathbf{v}_{r_N})(\tau_i) - T^2 \sum_{k=0}^N \alpha_k K(\tau_i, \tau_k) \left( \mathbf{a}(\mathbf{r}_k, \mathbf{u}_0, \mathbf{p}_0) + \frac{\partial \mathbf{a}(\mathbf{r}_k, \mathbf{u}_0, \mathbf{p}_0)}{\partial \mathbf{u}} \delta \mathbf{u} + \frac{\partial \mathbf{a}(\mathbf{r}_k, \mathbf{u}_0, \mathbf{p}_0)}{\partial \mathbf{p}} \delta \mathbf{p} + \frac{\partial \mathbf{a}(\mathbf{r}_k, \mathbf{u}_0, \mathbf{p}_0)}{\partial \mathbf{r}_k} \mathbf{v}_{r_k} \right) \quad (1)$$

$$\dot{\mathbf{r}}(\tau_i) + \mathbf{v}_r(\tau_i) = \frac{(\mathbf{r}_N + \mathbf{v}_{r_N}) - (\mathbf{r}_0 + \mathbf{v}_{r_0})}{T} + T \sum_{k=0}^N \beta_k \frac{\partial K(\tau_i, \tau_k)}{\partial \tau} \left( \mathbf{a}(\mathbf{r}_k, \mathbf{u}_0, \mathbf{p}_0) + \frac{\partial \mathbf{a}(\mathbf{r}_k, \mathbf{u}_0, \mathbf{p}_0)}{\partial \mathbf{u}} \delta \mathbf{u} + \frac{\partial \mathbf{a}(\mathbf{r}_k, \mathbf{u}_0, \mathbf{p}_0)}{\partial \mathbf{p}} \delta \mathbf{p} + \frac{\partial \mathbf{a}(\mathbf{r}_k, \mathbf{u}_0, \mathbf{p}_0)}{\partial \mathbf{r}_k} \mathbf{v}_{r_k} \right) \quad (2)$$

with integral kernel,

$$K(\tau, \tau') = \begin{cases} \tau(1 - \tau'), & \tau \leq \tau' \\ \tau'(1 - \tau), & \tau \geq \tau' \end{cases} \quad (3)$$

where  $\mathbf{r}_k(\tau)$  stands for the satellite's position observation at normalize time  $\tau$  and  $\mathbf{v}_r(\tau)$  is

correction vector,  $\alpha_k$  is integration coefficient,  $N$  is maximum index of epochs,  $T$  is arc length. The component  $\mathbf{a}$  denotes the force acting on unit mass satellite.  $\mathbf{u}$  is the vector of the geopotential coefficients and  $\mathbf{p}$  is the vector of the accelerometer parameters.  $\mathbf{u}_0$  and  $\mathbf{p}_0$  are initial values of  $\mathbf{u}$  and  $\mathbf{p}$ , and  $\delta\mathbf{u}$  and  $\delta\mathbf{p}$  are their corrections. The observation equation for range-rate measurement  $\dot{\rho}(\tau_i)$  is modelled as follows,

$$\dot{\rho}(\tau_i) = \mathbf{e}_{AB}^T(\tau_i) \cdot (\dot{\mathbf{r}}_B(\tau_i) - \dot{\mathbf{r}}_A(\tau_i)) = \mathbf{f}(\mathbf{r}_A(\tau_i), \mathbf{r}_B(\tau_i), \mathbf{u}, \mathbf{p}) \quad (4)$$

where  $\mathbf{e}_{AB}(\tau_i)$  is the unit vector of line-of-sight direction,  $\mathbf{r}_A(\tau_i)$  and  $\mathbf{r}_B(\tau_i)$  are the position vectors for both satellites,  $\dot{\mathbf{r}}_A(\tau_i)$  and  $\dot{\mathbf{r}}_B(\tau_i)$  stand for the velocity vectors for the twin satellites. Implementing the linearization of Eq. (4), we conduct the linearized observation equation for the range-rate measurement as follows (Chen et al. 2015a),

$$\begin{aligned} \dot{\rho}(\tau_i) + v_{\dot{\rho}}(\tau_i) = & \mathbf{f}(\mathbf{r}_A(\tau_i), \mathbf{r}_B(\tau_i), \mathbf{u}_0, \mathbf{p}_{A0}, \mathbf{p}_{B0}) + \\ & \frac{\partial \mathbf{f}}{\partial \mathbf{u}} \delta \mathbf{u} + \frac{\partial \mathbf{f}}{\partial \mathbf{p}_A} \delta \mathbf{p}_A + \frac{\partial \mathbf{f}}{\partial \mathbf{p}_B} \delta \mathbf{p}_B + \sum_{i=0}^N \left( \frac{\partial \mathbf{f}}{\partial \mathbf{r}_{A_i}} v_{r_{A_i}} + \frac{\partial \mathbf{f}}{\partial \mathbf{r}_{B_i}} v_{r_{B_i}} \right) \end{aligned} \quad (5)$$

where  $v_{\dot{\rho}}(\tau_i)$  is the correction for the range-rate measurement  $\dot{\rho}(\tau_i)$ ,  $\delta\mathbf{p}_A$  and  $\delta\mathbf{p}_B$  are the corrections of the accelerometer biases for GRACE A and GRACE B,  $v_{r_A}$  and  $v_{r_B}$  are the correction vectors for the twin satellites' orbits.

## 2.2 Treatment of non-conservative acceleration and attitude data

In the modified short arc approach proposed by Shen et al. (2013) and Chen et al. (2015a), the non-conservative acceleration and attitude data are taken as error-free observations. The component  $\mathbf{a}$  is composed of the conservative force  $\mathbf{a}_g$  and the non-conservative force  $\mathbf{a}_{ng}$ , which can be expressed as follows,

$$\mathbf{a}(\mathbf{r}_k, \mathbf{a}_s, \mathbf{q}, \mathbf{u}, \mathbf{p}) = \mathbf{a}_g(\mathbf{r}_k, \mathbf{u}) + \mathbf{a}_{ng}(\mathbf{a}_s, \mathbf{q}, \mathbf{p}) \quad (6)$$

where the conservative force  $\mathbf{a}_g$  can be calculated from models using  $\mathbf{r}_k$  and  $\mathbf{u}$ . The non-conservative force  $\mathbf{a}_{ng}$  is computed from the attitude data  $\mathbf{q} = (q_1 \ q_2 \ q_3 \ q_4)$  and the accelerometer measurement  $\mathbf{a}_s$  measured in the Science Reference Frame as follows (Bettadpur 2012),

$$\mathbf{a}_{ng}(\mathbf{a}_s, \mathbf{q}, \mathbf{p}) = \mathbf{C}(\mathbf{q})^T (\mathbf{S} \mathbf{a}_s + \mathbf{p}) \quad (7)$$

where  $\mathbf{S}$  is the accelerometer scale that is not estimated and is taken from Bettadpur (2009), and  $\mathbf{p}$  represents the accelerometer bias that is estimated per hour.  $\mathbf{C}(\mathbf{q})$  denotes rotation matrix from the inertial system to the Science Reference Frame, which can be expressed as follows,

$$\mathbf{C}(\mathbf{q}) = \begin{pmatrix} q_1^2 - q_2^2 - q_3^2 + q_4^2 & 2(q_1q_2 + q_3q_4) & 2(q_1q_3 - q_2q_4) \\ 2(q_1q_2 - q_3q_4) & -q_1^2 + q_2^2 - q_3^2 + q_4^2 & 2(q_2q_3 + q_1q_4) \\ 2(q_1q_3 + q_2q_4) & 2(q_2q_3 - q_1q_4) & -q_1^2 - q_2^2 + q_3^2 + q_4^2 \end{pmatrix} \quad (8)$$

To take the errors of the non-conservative acceleration and attitude measurements into account, we introduce correction terms to both the non-conservative acceleration and attitude measurements (namely  $\mathbf{v}_{a_s}$  and  $\mathbf{v}_q$ ) as follows,

$$\begin{cases} \mathbf{a}_s = \mathbf{a}_s^k + \mathbf{v}_{a_s} \\ \mathbf{q} = \mathbf{q}^k + \mathbf{v}_q \end{cases} \quad (9)$$

where  $\mathbf{a}_s^k$  and  $\mathbf{q}^k$  represent the non-conservative acceleration and attitude measurements at  $k$ -th epoch. Using Eqs. (1) and (9), we derive the observation equation for the orbit measurements, which is expressed as,

$$\mathbf{r}(\tau_i) + \mathbf{v}_r(\tau_i) = (\mathbf{r}_0 + \mathbf{v}_{r_0})(1 - \tau_i) + (\mathbf{r}_N + \mathbf{v}_{r_N})(\tau_i) - T^2 \sum_{k=0}^N \alpha_k K(\tau_i, \tau_k) \left( \begin{aligned} & \mathbf{a}(\mathbf{r}_k, \mathbf{a}_s^k, \mathbf{q}^k, u_0, \mathbf{p}_0) + \frac{\partial \mathbf{a}(\mathbf{r}_k, \mathbf{a}_s^k, \mathbf{q}^k, u_0, \mathbf{p}_0)}{\partial u} \delta u + \frac{\partial \mathbf{a}(\mathbf{r}_k, \mathbf{a}_s^k, \mathbf{q}^k, u_0, \mathbf{p}_0)}{\partial \mathbf{p}} \delta \mathbf{p} + \\ & \frac{\partial \mathbf{a}(\mathbf{r}_k, \mathbf{a}_s^k, \mathbf{q}^k, u_0, \mathbf{p}_0)}{\partial \mathbf{r}_k} \mathbf{v}_{r_k} + \frac{\partial \mathbf{a}(\mathbf{r}_k, \mathbf{a}_s^k, \mathbf{q}^k, u_0, \mathbf{p}_0)}{\partial \mathbf{a}_s^k} \mathbf{v}_{a_s^k} + \frac{\partial \mathbf{a}(\mathbf{r}_k, \mathbf{a}_s^k, \mathbf{q}^k, u_0, \mathbf{p}_0)}{\partial \mathbf{q}^k} \mathbf{v}_{q^k} \end{aligned} \right) \quad (10)$$

Similarly, the linearized observation equation for the range-rate data can be conducted as follows,

$$\dot{\rho}(\tau_i) + \mathbf{v}_{\dot{\rho}}(\tau_i) = \mathbf{f}(\mathbf{r}_A(\tau_i), \mathbf{r}_B(\tau_i), \mathbf{a}_{s_A}, \mathbf{a}_{s_B}, \mathbf{q}_A, \mathbf{q}_B, u_0, \mathbf{p}_{A0}, \mathbf{p}_{B0}) + \left( \begin{aligned} & \frac{\partial \mathbf{f}}{\partial \mathbf{r}_{A_i}} \mathbf{v}_{r_{A_i}} + \frac{\partial \mathbf{f}}{\partial \mathbf{r}_{B_i}} \mathbf{v}_{r_{B_i}} + \frac{\partial \mathbf{f}}{\partial \mathbf{a}_{s_A}^i} \mathbf{v}_{a_{s_A}^i} + \\ & \frac{\partial \mathbf{f}}{\partial u} \delta u + \frac{\partial \mathbf{f}}{\partial \mathbf{p}_A} \delta \mathbf{p}_A + \frac{\partial \mathbf{f}}{\partial \mathbf{p}_B} \delta \mathbf{p}_B + \sum_{i=0}^N \left( \begin{aligned} & \frac{\partial \mathbf{f}}{\partial \mathbf{a}_{s_B}^i} \mathbf{v}_{a_{s_B}^i} + \frac{\partial \mathbf{f}}{\partial \mathbf{q}_A^i} \mathbf{v}_{q_A^i} + \frac{\partial \mathbf{f}}{\partial \mathbf{q}_B^i} \mathbf{v}_{q_B^i} \end{aligned} \right) \end{aligned} \right) \quad (11)$$

where the subscripts A and B denote the quantities related to GRACE A and GRACE B. Since the attitude quaternion elements  $q_1, q_2, q_3$  and  $q_4$  are not independent, a constraint equation for the quaternion elements is introduced as follows,

$$\mathbf{q}^T \mathbf{q} = 1 \quad (12)$$

Inserting Eq. (9) into (12) leads to the observation equation bellow for the attitude observations,

$$2(\mathbf{q}^k)^T \mathbf{v}_{q^k} = 1 - (\mathbf{q}^k)^T \mathbf{q}^k \quad (13)$$

To simplify the forms of the above observation equations, the observation equations including (10), (11) and (13) at  $j$ -th arc can be summarized as follows,

$$\mathbf{A}_j \mathbf{x}_j + \mathbf{B}_j \mathbf{v}_j = \mathbf{l}_j \quad (14)$$

in which,  $\mathbf{x}_j = (\delta \boldsymbol{\mu}^T, \delta \mathbf{p}_{A_j}^T, \delta \mathbf{p}_{B_j}^T)^T$  denotes the unknown parameters to be estimated, and

$\mathbf{v}_j = (\mathbf{v}_{r_A}^T, \mathbf{v}_{r_B}^T, \mathbf{v}_{a_{s_A}}^T, \mathbf{v}_{a_{s_B}}^T, \mathbf{v}_{q_A}^T, \mathbf{v}_{q_B}^T, \mathbf{v}_{\rho}^T)^T$  is the correction vector for all observations (including the orbits, the non-conservative accelerations, and the attitudes, as well as the inter-satellite range-rates), and  $\mathbf{l}_j$  is residual vector. The design matrix  $\mathbf{A}_j$  with full column rank includes partial derivatives with respect to the vector of the unknown parameters  $\mathbf{x}_j$ , which is presented in the observation equations (10) and (11). The design matrix  $\mathbf{B}_j$  with full row rank is calculated from the partial derivatives with respect to the correction vector  $\mathbf{v}_j$  as shown in the observation equations **containing (10), (11) and (13)**. Therefore, the matrix  $(\mathbf{B}_j \mathbf{Q}_j \mathbf{B}_j^T)$  is invertible and the sub-normal equation of each arc for solving the unknowns can be derived by using a weighted least adjustment by minimizing  $\mathbf{v}_j^T \mathbf{Q}_j^{-1} \mathbf{v}_j$ ,

$$\left( \mathbf{A}_j^T (\mathbf{B}_j \mathbf{Q}_j \mathbf{B}_j^T)^{-1} \mathbf{A}_j \right) \begin{pmatrix} \delta \mathbf{u} \\ \delta \mathbf{p}_{A_j} \\ \delta \mathbf{p}_{B_j} \end{pmatrix} = \mathbf{A}_j^T (\mathbf{B}_j \mathbf{Q}_j \mathbf{B}_j^T)^{-1} \mathbf{l}_j \quad (15)$$

in which  $\mathbf{Q}_j$  is the priori variance-covariance matrix. Because the orbit, range-rate, attitude and non-conservative acceleration observations are independent and the temporal correlation of each type of observations is neglected in our computation, the priori variance-covariance matrix  $\mathbf{Q}_j$  is a diagonal matrix; its diagonal elements are computed using the priori accuracies of the measurements (including the orbits, range-rates, attitudes, and non-conservative accelerations). The computational burden of matrix  $(\mathbf{B}_j \mathbf{Q}_j \mathbf{B}_j^T)$  is associated with the arc length, thus longer arc length will cause higher computational burden. Once the parameters are determined, the correction vector can be solved by,

$$\mathbf{v}_j = \mathbf{Q}_j \mathbf{B}_j^T (\mathbf{B}_j \mathbf{Q}_j \mathbf{B}_j^T)^{-1} \left( \mathbf{l}_j - \mathbf{A}_j \begin{pmatrix} \delta \mathbf{u} \\ \delta \mathbf{p}_{A_j} \\ \delta \mathbf{p}_{B_j} \end{pmatrix} \right) \quad (16)$$

Since only the geopotential coefficients  $\delta \mathbf{u}$  are solved in our final normal equation, the arc-specific parameters  $\delta \mathbf{p}_A$  and  $\delta \mathbf{p}_B$  are first eliminated, then all sub-normal equations are merged into the final normal equation. Here we should point out that the accelerometer biases for the twin satellites are estimated per hour and all the correction terms for the orbit, range-rate, attitude, and non-conservative acceleration measurements are solved per epoch.

### 3. Effects of non-conservative acceleration and attitude observation errors

The above algorithms of estimating the errors of the non-conservative acceleration and attitude measurements are implemented in the SAtellite Gravimetry Analysis Software (SAGAS) developed by the Tongji University for the determination of the gravity field from satellite-based observations. The background force models as shown in Chen et al. (2015a; 2015d) have been used in the SAGAS software for removing the non-gravitational perturbations, namely the N-Body

perturbations (International Earth Rotation Service (IERS) 2010 conventions), the solid Earth tides (IERS 2010 conventions), the ocean tides (EOT11a,  $N_{\max}=80$ ), the solid Earth pole tides (IERS 2010 conventions,  $C_{21}$  &  $S_{21}$ ), the ocean pole tides (Desai model,  $N_{\max}=30$ ), the atmosphere and oceanic variability (AOD1B RL05,  $N_{\max}=100$ ), and the general relativistic perturbations (IERS 2010 conventions). Three accelerometer biases in three axis directions are estimated every hour for each satellite (Dahle et al. 2012). Similar to Chen et al. (2015a) in deriving the Tongji-GRACE01 monthly solutions, two hour arcs are used to perform orbit integration by using the above force models. The GRACE Level-1B measurements from Jet Propulsion Laboratory (JPL), containing the reduced-dynamic orbits, attitudes, non-conservative accelerations of GRACE A and GRACE B together with the inter-satellite range-rates, are used for GRACE monthly solution determination. The orbit data have a sampling rate of 5 seconds and an accuracy of about 2 cm (Kang et al. 2006a, 2006b), the range-rate data with an accuracy of about  $0.2\mu\text{m/s}$  (Beutler et al. 2010) are also sampled with 5 seconds. The GRACE Level-1B accelerometer data from JPL are with a sampling rate of 1 second and a claimed accuracy of around  $10^{-10}\text{m/s}^2$  within the bandwidth of  $2 \times 10^{-4} - 0.1\text{Hz}$  (Kang et al. 2006b), and they are re-sampled with 5 seconds to keep consistent with the integration step (5s). The attitude measurements in terms of quaternion product QSA1B from the onboard star cameras are collected every 5 seconds and with an accuracy of around  $100\mu\text{rad}$  (Han et al. 2006). Since the data gaps frequently occur in attitude and non-conservative acceleration observations, the interpolation algorithms proposed by Wu et al. (2006) are used in our data processing. When the reduced-dynamic orbits are used, the derived gravity field is theoretically biased towards the priori gravity field for generating the reduced-dynamic orbits. Nevertheless, when the K-band range-rate measurements are used in computing gravity field, the impacts of the reduced-dynamic orbits are not significant (Liu et al. 2010; Chen et al. 2015b).

In order to study the effects of the non-conservative acceleration and attitude observation errors on the gravity field solution, we compute four solutions from the GRACE measurements of Jan. 2008 (including the reduced-dynamic orbits, inter-satellite range-rates, attitudes and non-conservative accelerations) using the following ways: (a) without estimating the acceleration and attitude data errors; (b) only estimating the acceleration data errors; (c) only estimating the attitude data errors; and (d) estimating the acceleration and attitude data errors. The resulting gravity field solutions in terms of geoid degree variances are displayed in Figure 1, where the degree variances (especially for high degrees) are reduced by either estimating the acceleration data errors or estimating the attitude data errors. The cumulative geoid degree variance up to degree and order 60 is 1.47 mm for the case of estimating the acceleration and attitude data errors, suggesting 40.8% of improvement in terms of cumulative geoid degree variance is



achieved compared to the case of treating them as error-free data (with cumulative geoid degree variance of 2.07 mm). From Figure 1 we can conclude that the modelling of the acceleration data errors is more important than the modelling of attitude data errors for improving the gravity field solution, although the modelling of attitude data errors also has contributions to the final gravity field solution.

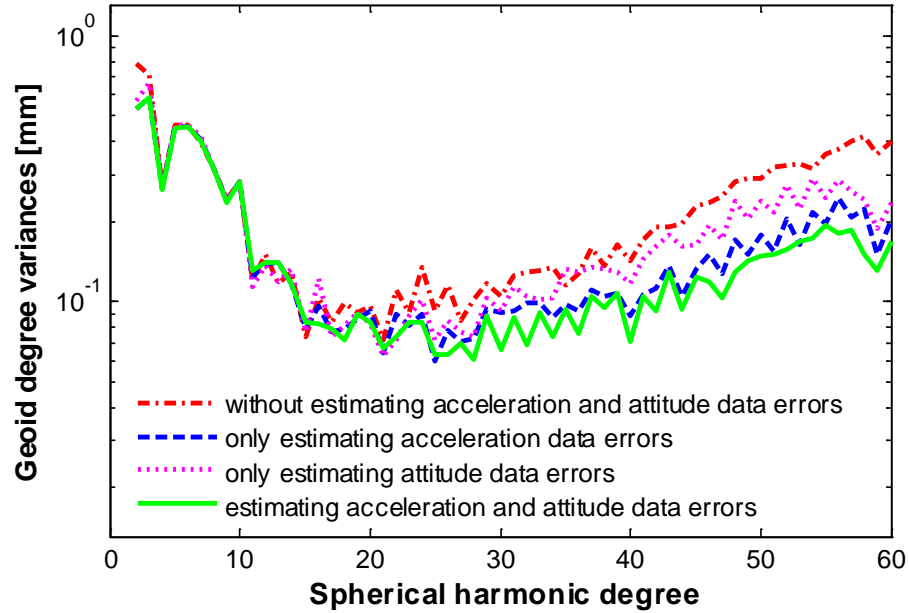


**Figure 1** Effects of acceleration and attitude data errors in terms of geoid degree variances (EIGEN6C2 acts as the mean field).

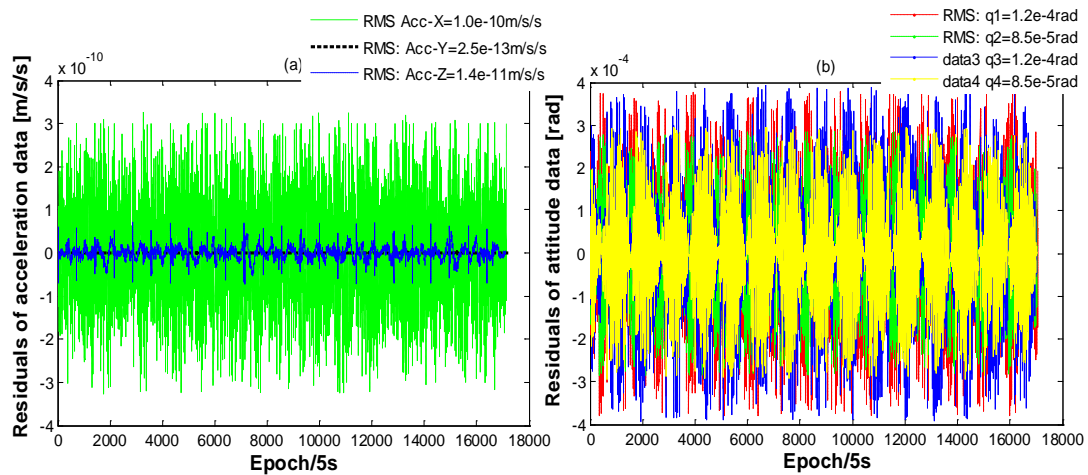


**Figure 2** Corrections of the acceleration (a) and attitude (b) data of GRACE-A on 1 January 2008.

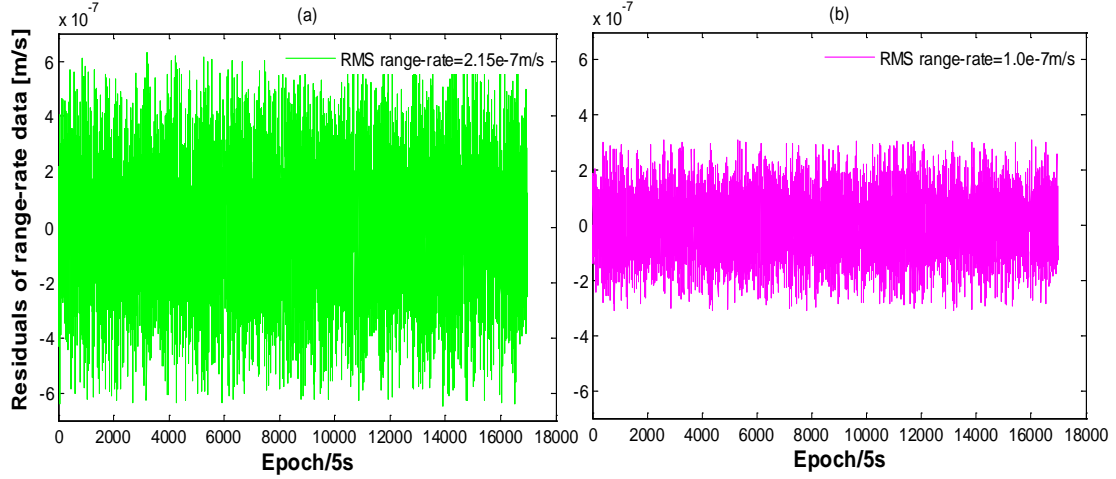


**Figure 3** Postfit residuals of the range-rate data on 1 January 2008 without (a) and with (b) estimating the attitude and non-conservative acceleration data errors.

To show the properties of the acceleration and attitude errors, we present the corrections for the acceleration and attitude data of GRACE-A on 1 Jan. 2008 in Figure 2 using Eq. (16). The RMS value of the solved acceleration corrections in X direction is  $10^{-10}\text{m/s}^2$  (same as the official claimed accuracy), while the RMS values of the acceleration corrections in Y and Z directions are much smaller than the official accuracy. However, the estimated acceleration errors in the Y and Z directions are not reliable since the K-band range-rate measurements are only sensitive to the X direction. The RMS values of the solved attitude corrections are about  $1.2 \times 10^{-4}\text{rad}$  for  $q_1$  and  $q_3$ , and  $8.5 \times 10^{-5}\text{rad}$  for  $q_2$  and  $q_4$ , which are close to the claimed accuracy. The postfit residuals of the range-rate data on 1 January 2008 with and without modelling the attitude and non-conservative acceleration data errors are given in Figure 3, which confirms that the modelling of the attitude and non-conservative acceleration data errors can benefit reduction of the postfit residuals of the range-rate measurements.

#### 4. Tongji-GRACE02 monthly gravity field solution

The unconstrained monthly gravity field models called Tongji-GRACE02 spanning Jan. 2003 to Dec. 2012 are estimated up to degree and order 60, and the gravitational effects beyond degree and order 60 are removed with ITG-GRACE2010s model. Since the non-conservative acceleration and attitude observation errors have been modelled, Tongji-GRACE02 models are anticipated to have less north-south stripes. Figure 4 shows the mass changes (the subtracted mean field is the average of CSR RL05 over the period Jan. 2003 to Dec. 2012) over global ocean derived from CSR RL05 and Tongji-GRACE02 models for the months Jan. 2003, Sept. 2004 and Jan. 2006, in which a Gaussian smoothing (Jekeli, 1981) with a radius of 300 km is applied to remove high frequency noise in the GRACE estimates and no decorrelation filtering is used. The reason for not using the decorrelation filtering here is that the north-south stripes will be more visible in this case. CSR RL05 is developed by Center for Space Research (CSR) complete to degree and order 96. All of the

solutions are truncated to degree and order 60 in order to ensure a fair comparison between Tongji-GRACE02 and the others in this paper, since Tongji-GRACE02 is only complete to degree and order 60, which does not contain high degree signals. Certainly such truncation may lead to omission of high frequency signals, but the higher degree coefficients of GRACE solution is dominated by noise (Wahr et al. 2004). In particular, the  $C_{20}$  values are replaced with those from satellite laser ranging (Cheng and Tapley 2004) and the degree one coefficients are substituted with those from Swenson et al. (2008). The reason to choose these three months for comparison is that Jan. 2003 stands for the month with poor data quality and large data gaps, Sept. 2004 is the month with sparse ground track coverage, and Jan. 2006 represents the month with denser ground track coverage and better data quality. The north-south stripes of Tongji-GRACE02 models in Jan. 2003 and Sept. 2004 are less than those of CSR RL05 models, since the observation errors of the non-conservative accelerations and attitudes are not modelled by CSR RL05 solutions, which means that our algorithms of modelling the observation errors of the non-conservative accelerations and attitudes can effectively improve the quality of the solved gravity field model. However, the difference of the north-south stripes between CSR RL05 and Tongji-GRACE02 become small for the month Jan. 2006.

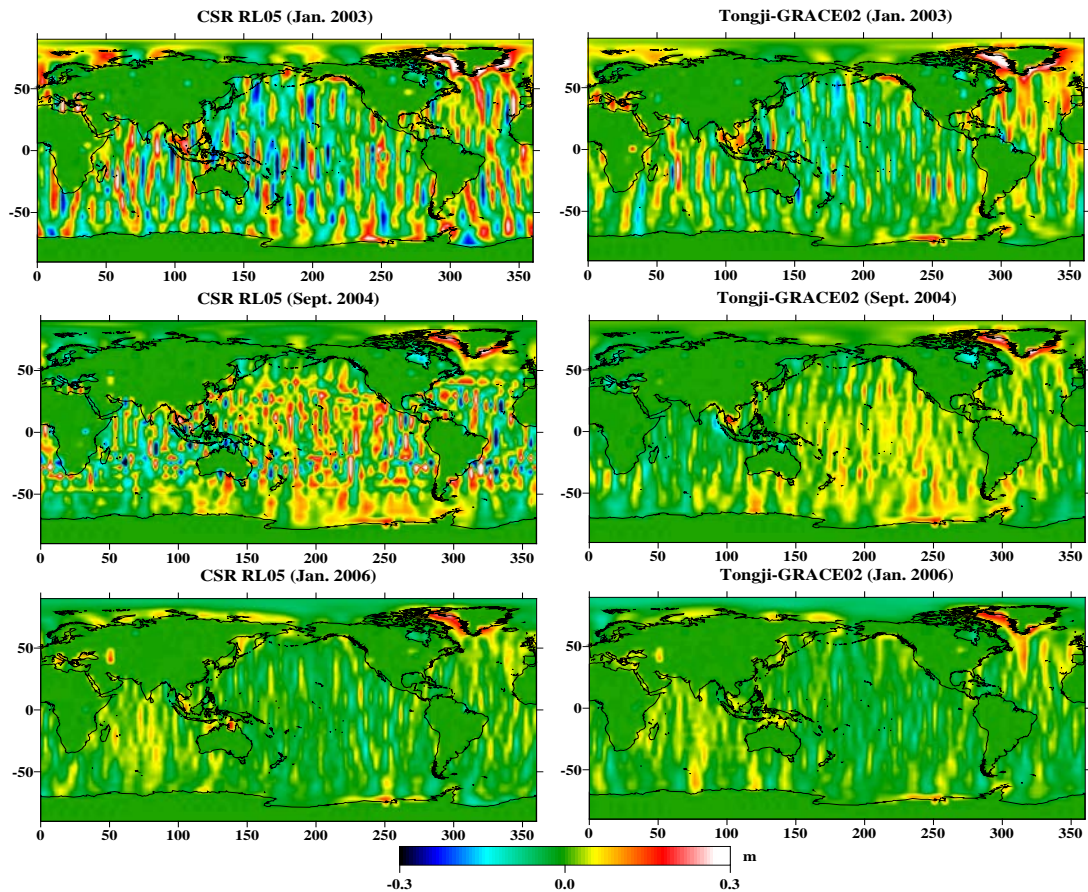


**Figure 4** Mass changes in terms of equivalent water height (EWH) of Jan. 2003, Sept. 2004 and Jan. 2006 inferred from CSR RL05 and Tongji-GRACE02 models.

The comparisons of geoid degree variances with respect EIGEN6C2 between Tongji-GRACE02 and CSR RL05 shown in Figure 5 further confirm that Tongji-GRACE02 has a significant reduction of noise at high degrees for the poor months Jan. 2003 and Sept. 2004. The noise reduction is not significant for the month Jan. 2006 with good data quality and ground track coverage. **One may argue that the improvement of Tongji-GRACE02 compared to CSR RL05 is caused by the short arc approach used for Tongji-GRACE02, since CSR RL05 is based on dynamic approach. Here, we further add ITG-Grace2010 monthly solutions (Mayer-Gürr et al. 2010) generated by the short arc approach as well for the same three months to Figure 5 to address this issue. The conclusions do not change from the comparisons between ITG-Grace2010 and Tongji-GRACE02 monthly solutions.**

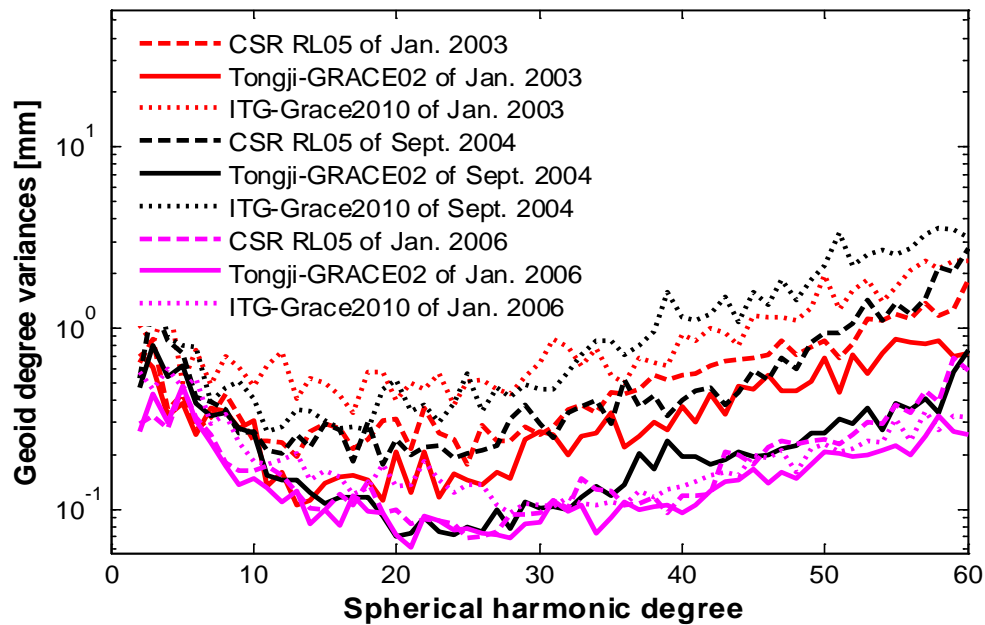


**Figure 5** Geoid degree variances of CSR RL05 and Tongji-GRACE02 for the months Jan. 2003, Sept. 2004 and Jan. 2006 with respect to EIGEN6C2.

Because directly quantifying the north-south striping errors over ocean is complicated, we indirectly evaluate the north-south striping errors by comparing the mean mass changes and the RMS values over global ocean from Tongji-GRACE02 and the official solutions (i.e. CSR RL05, GFZ RL05a, and JPL RL05) for the period Jan. 2003 to Dec. 2012, in which GFZ RL05a and JPL RL05 were developed by GeoForschungsZentrum Potsdam (GFZ) and JPL. The GFZ RL05a and JPL 05 with the maximum degree and order 90 and 60, should be truncated to degree and order 60. The four GRACE solutions are all filtered with a 300 km Gaussian smoothing in this comparison. The mean mass changes and RMS values of the residuals after removing dominant seasonal terms (the bias, acceleration, annual, semiannual, and the S2 alias terms) for these four GRACE solutions are presented in Figure 6. We can find from Figure 6(a) that the mean mass change

from Tongji-GRACE02 agrees well with those from the official solutions. Since temporal tidal and non-tidal effects over ocean areas are mostly removed by the background force models during the determination of the GRACE solutions and the dominant seasonal terms estimated are subtracted, the residuals over ocean can be approximately treated as the noise of the GRACE solutions besides the remaining errors of the background force models (Kurtenbach et al. 2009, Chen et al. 2014). Figure 6(b) shows that Tongji-GRACE02 has the least mean RMS value among the four solutions for the whole time series except for a few months in 2011. The mean RMS values of all the months are 4.6 cm, 6.6 cm, 5.4 cm, and 3.7 cm for CSR RL05, GFZ RL05a, JPL RL05 and Tongji-GRACE02, indicating that Tongji-GRACE02 solution reduces the RMS of about 24%, 78% and 46% over ocean when comparing to CSR RL05, GFZ RL05a and JPL RL05.

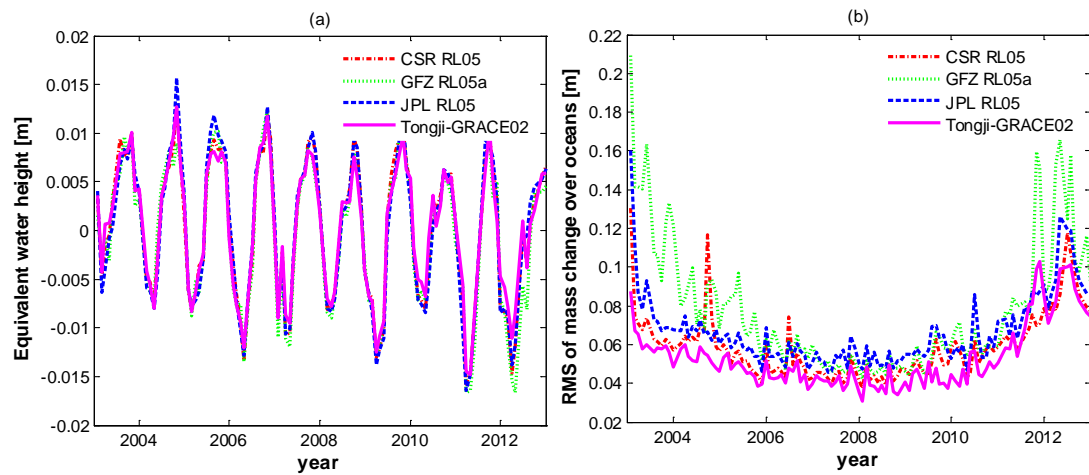


**Figure 6** (a): The mass change series; (b): RMS value series over ocean derived from CSR RL05, GFZ RL05a, JPL RL05 and Tongji-GRACE02 for the period Jan. 2003 to Dec. 2012.

## 5. Comparisons of GRACE monthly models

This section first discusses the global mass signals from various GRACE solutions. Then the signal powers and noise in three continents with strong signals (India, South America and Southeast Asia) and two large-scale river basins (Mississippi and Congo River basins) as well as four deserts (Australia, Kalahari, Karakum and Thar) from Tongji-GRACE02 and the official solutions for the period Jan. 2003 to Dec. 2012 are analyzed. The regional kernel is defined as 1 inside the region and 0 outside the region. The average field of CSR RL05 for the period Jan. 2003 to Dec. 2012 is taken as the reference field in the computation of mass changes.

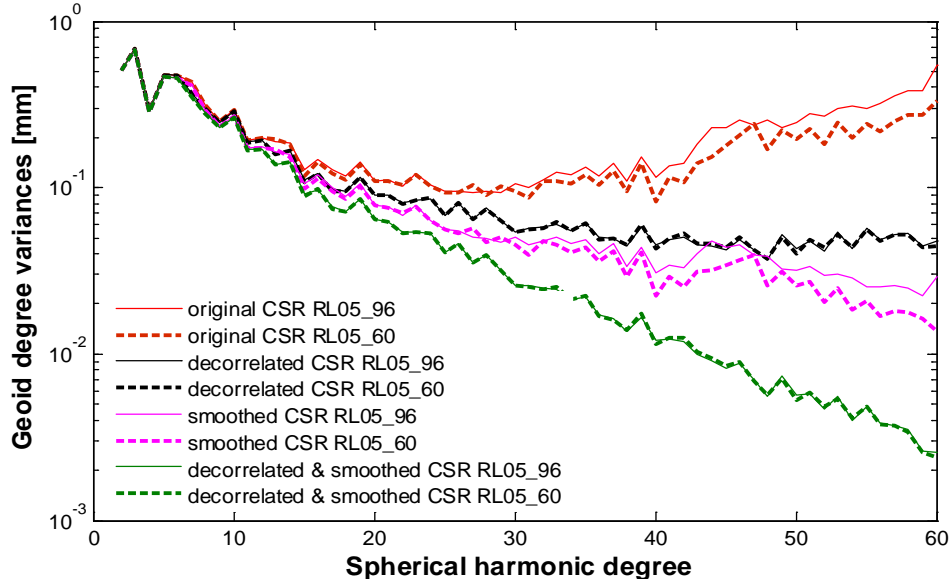


**Figure 7** Impacts of truncation, decorrelation filtering and smoothing in terms of geoid degree variances.

The original GRACE solutions (especially the high degree coefficients) are dominated by noise (especially the north-south stripes) to so a great extent that directly computing the mass changes for a particular region is almost impossible, thus, the original GRACE solutions are usually truncated to a maximum degree in the gravity field recovery and processed with some smoothing or filtering methods. The presence of the north-south stripes is caused by a high correlation between odd and even degree coefficients of the original GRACE solutions for the same order (Swenson and Wahr, 2006). As suggested by Chen et al (2009a), a  $P_4M_6$  decorrelation filtering is applied to reduce the effects of the north-south stripes of the original GRACE solutions in this study. The key to the  $P_4M_6$  decorrelation filtering is to subtract a 4 degree fit polynomial from the odd and even degree components for the residual coefficients with the same order from 6 to the maximum degree. Based on the  $P_4M_6$  decorrelation filtering, the GRACE solutions are smoothed with a 300 km Gaussian smoothing in order to suppress high frequency noise. Here, we investigate the impacts of the truncation and  $P_4M_6$  decorrelation filtering as well as 300 km Gaussian smoothing on noise reductions in terms of geoid degree variances by using two GRACE solutions of Jan. 2008 provided by CSR. One is with the maximum degree 96 and is truncated to degree 60 in this paper, and the other is purely up to degree and order 60. The results illustrated in Figure 7 come to the conclusions as follows: (1) The truncation in the gravity field estimation leads to the noise reductions of high degree coefficients. (2) The  $P_4M_6$  decorrelation filtering reduces much more noise than the 300 km Gaussian smoothing. (3) The difference due to the truncation vanishes when using the  $P_4M_6$  decorrelation filtering.

However, such truncation and filtering as well as smoothing certainly lead to leakage effects, which are corrected by leakage biases (Klees et al. 2007; Velicogna and Wahr 2013) when



analyzing the mass changes in the two river basins and three continents. The leakage biases are estimated from the GLDAS grid data (Global Land Data Assimilation System data, Rodell et al. 2004) by using the same truncation and smoothing as well as filtering as GRACE models. To separate the noise from the signal powers in the Mississippi and Congo River basins for the GRACE solutions, the processing strategies are taken as follows:

(1) Dominant seasonal terms (including the bias, **trend**, acceleration, annual, seminnual, octennial, quadrennial, and the S2 alias components) for the time series of the mass changes computed from the filtered solutions and leakage biases are estimated by using a least squares adjustment. (2) The dominant mass change signals are constructed by using the estimated dominant seasonal terms. In such a way, the signal power for each GRACE solution can be quantified by the mean amplitude (including the annual, seminnual, octennial and quadrennial as well as S2 amplitudes) of the dominant seasonal signals. (3) The noise of the GRACE solutions is evaluated by two parts. One is the RMS values of the residuals of the filtered solutions (by subtracting the dominant seasonal signals from the filtered mass changes), which are usually treated as the noise level of the filtered solutions (Chen et al. 2014). The other one is the RMS values of the residuals of the unfiltered (or original) solutions (by subtracting the dominant seasonal signals from the original mass changes), which are interpreted as the noise level of the original solutions in the following text. For the case of the selected continents (i.e. India, South America and Southeast Asia), the octennial and quadrennial terms are not considered in the estimation of the dominant seasonal signals and the computation of the mean amplitudes. **We should mention here that the noise levels of the GRACE solutions are evaluated by fitting the primary signal terms. If the other interesting signals significantly exist in the studied area, the noise levels will be not reasonable.**

## 5.1 Global mass change signals

The global mass changes in Oct. 2004 derived from CSR RL05, GFZ RL05a, JPL RL05 and Tongji-GRACE02 after applying the  $P_4M_6$  decorrelation filtering and the 300 km Gaussian smoothing are illustrated in Figure 8. It suggests that the main signals from Tongji-GRACE02 are consistent with those from CSR RL05, GFZ RL05a and JPL RL05, with strong signals in the Greenland, Antarctica, Amazon basin, South of Africa, and India, while the noise especially the north-south stripes of Tongji-GRACE02 is obviously less than that of the other solutions. However the mass change signals of Tongji-GRACE02 are also reduced, especially in the South America, India and Southeast Asia.

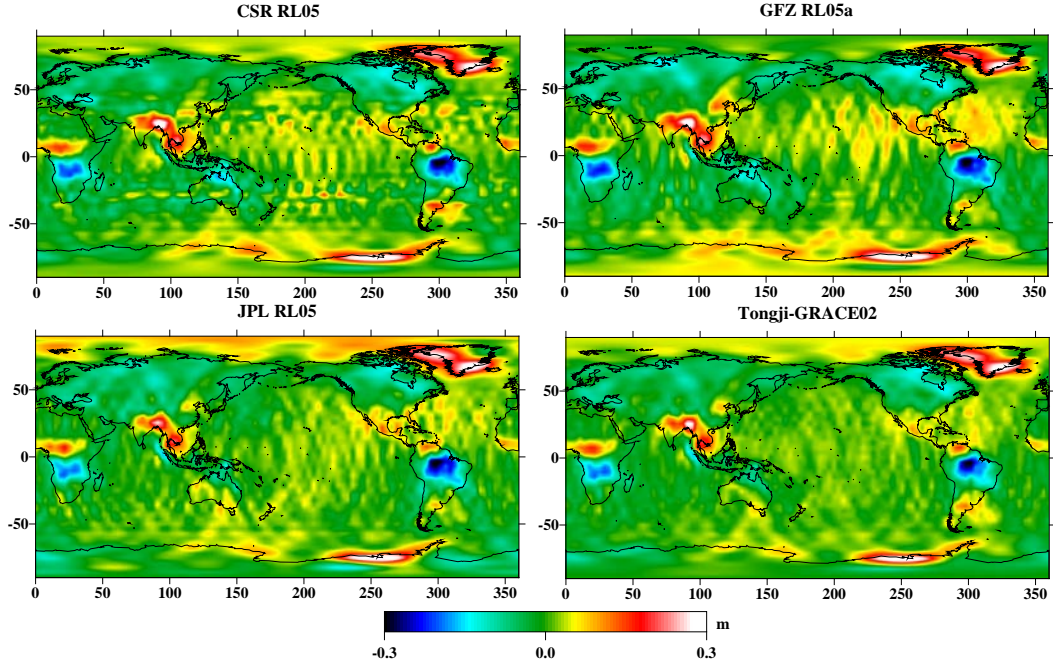


**Figure 8** Global mass variations (in EWH) derived from CSR RL05, GFZ RL05a, JPL RL05 and Tongji-GRACE02 of Oct. 2004 with a  $P_4M_6$  decorrelation filtering and a 300 km Gaussian smoothing.

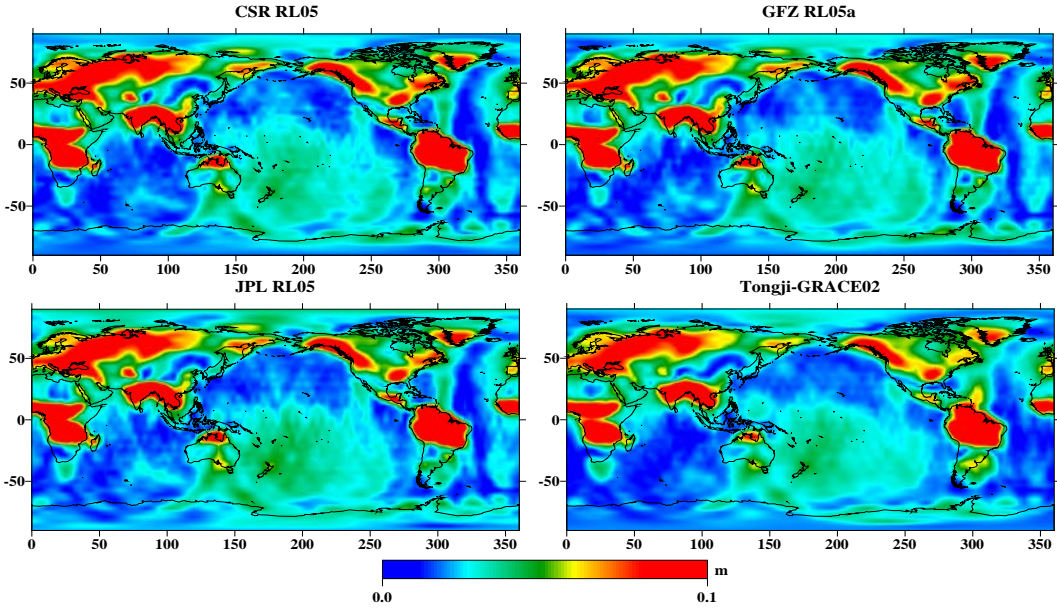


**Figure 9** Mean amplitudes of the global mass changes (in EWH) for different GRACE solutions using a 300 km Gaussian smoothing and a  $P_4M_6$  decorrelation filtering.

To further investigate the signals and noise of Tongji-GRACE02 with respect to other GRACE solutions, we compute the mean amplitudes of global mass changes by estimating the seasonal terms (including the bias, trend, acceleration, annual, semiannual and S2 terms) (Chen et al. 2009b) for these GRACE solutions spanning Jan. 2003 to Dec. 2012. When the GRACE solutions are processed with a  $P_4M_6$  decorrelation filtering and a 300 km Gaussian smoothing, the resulting mean amplitudes and the RMS values of the residuals are presented in Figures 9 and 10. Figure 9 suggests that the spatial pattern of the mean amplitude from Tongji-GRACE02 agrees



well with those from the official solutions. As mentioned in the previous section, the residuals over ocean areas can be approximately regarded as the noise level of the GRACE solutions (Kusche et al. 2009; Chen et al. 2014). Compared to the others, Tongji-GRACE02 has the least RMS values over ocean in Figure 10.

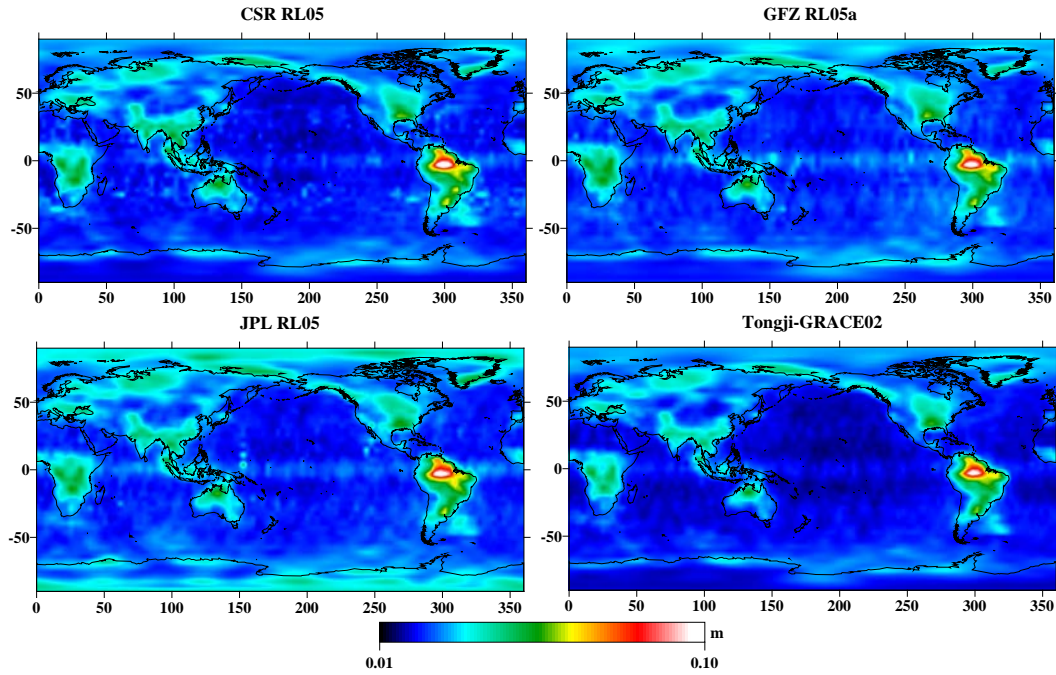


**Figure 10** RMS values of the residuals of the global mass changes (in EWH) for different GRACE solutions using a 300 km Gaussian smoothing and a  $P_4M_6$  decorrelation filtering.

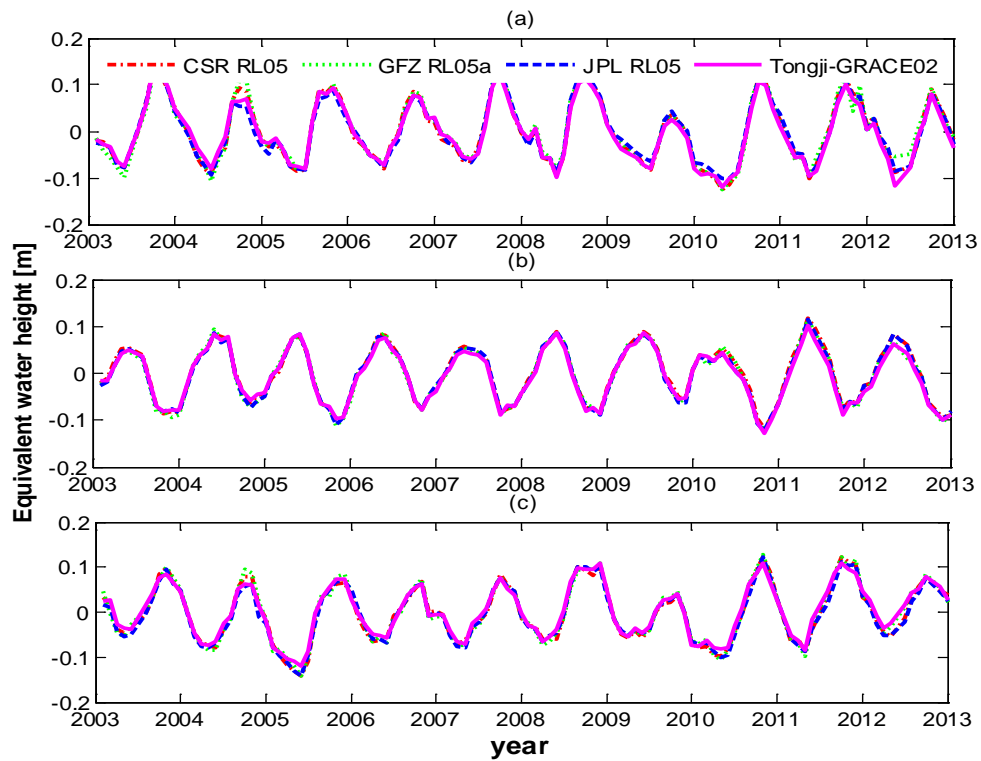


**Figure 11** Time series of mass changes (in EWH) inferred from CSR RL05, GFZ RL05a, JPL RL05, and

Tongji-GRACE02 over: (a) India; (b) South America; (c) Southeast Asia.

After processed with a  $P_4M_6$  decorrelation filtering and a 300 km Gaussian smoothing, the time series of mass changes in the India, South America and Southeast Asia derived from Tongji-GRACE02 and the three official GRACE solutions are demonstrated in Figure 11. It reveals that the time series of Tongji-GRACE02 shows a great agreement with those of the other three solutions. The mean amplitudes and the mean RMS values in the India, South America and Southeast Asia from the filtered and original GRACE solutions are presented in Table 1, which show that the reductions of RMS in Tongji-GRACE02 are more than the reductions of signal powers compared to CSR RL05.

**Table 1** The mean amplitudes and the mean RMS values of the residuals in the India, South America and Southeast Asia from the filtered and original solutions.

Region	Model and Reduction	Amplitude	RMS of residuals of filtered solution	RMS of residuals of original solution
India	CSR RL05	10.6 cm	4.0 cm	40.7 cm
	Tongji-GRACE02	10.0 cm	3.7 cm	31.0 cm
	Reduction	6%	9%	31%
South America	CSR RL05	13.2 cm	5.3 cm	52.9 cm
	Tongji-GRACE02	13.3 cm	5.0 cm	33.3 cm
	Reduction	0	6%	59%
Southeast Asia	CSR RL05	10.3 cm	4.9 cm	51.3 cm
	Tongji-GRACE02	9.6 cm	4.3 cm	31.8 cm
	Reduction	7%	14%	61%

## 5.2 Mass change signals in river basins

In order to investigate the capability of Tongji-GRACE02 to capture large seasonal signals, we compute the mass change time series in the Mississippi River basin of America and the Congo River basin of Africa (the regional boundaries for these basins are available on the website: <http://hydro.iis.u-tokyo.ac.jp/~taikan/TRIPDATA/TRIPDATA.html>) from the official solutions and Tongji-GRACE02 for the period Jan. 2003 to Dec. 2012. Figure 12 shows that the mass changes of these two basins from Tongji-GRACE02 agree well with those from the other solutions, which means that the large seasonal signals can be effectively picked up by Tongji-GRACE02. The correlation coefficients of the mass changes from CSR RL05, GFZ RL05a and JPL RL05 with respect to those from Tongji-GRACE02 are 0.99, 0.98 and 0.99 for the Congo River basin, while they are the same with 0.98 for the case of the Mississippi River basin. It indicates that Tongji-GRACE02 is strongly correlated with the others in the areas with strong seasonal signals. The signal powers of these two basins are quantified by the amplitudes estimated from CSR RL05 and Tongji-GRACE02, which are depicted in Figure 13. It demonstrates that the spatial patterns of the amplitudes from

CSR RL05 and Tongji-GRACE02 show a good agreement for both the Mississippi and Congo River basins.

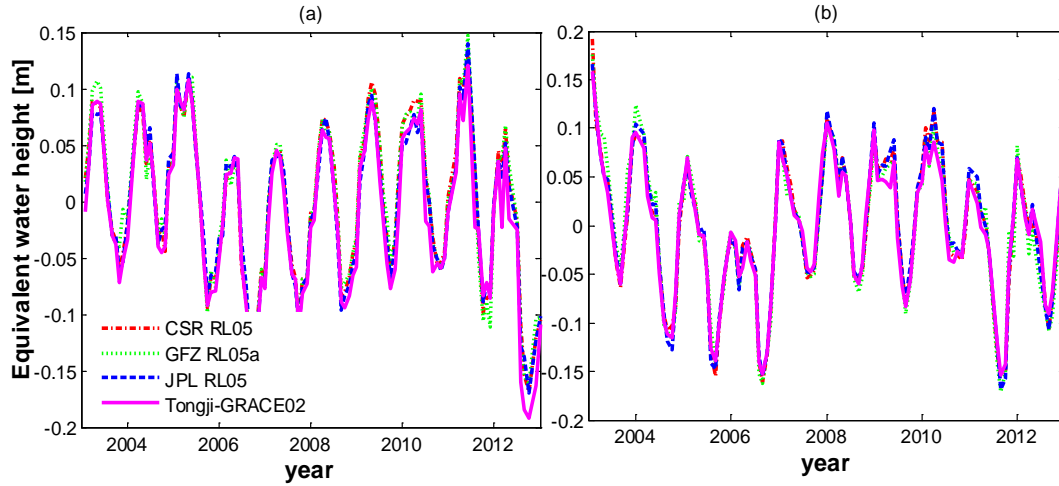


**Figure 12** Time series of mass changes (in EWH) inferred from CSR RL05, GFZ RL05a, JPL RL05, and Tongji-GRACE02 for the period Jan. 2003 to Dec. 2012 using a 300 km Gaussian smoothing and a  $P_4M_6$  decorrelation filtering in: (a) Mississippi River basin; (b) Congo River basin.

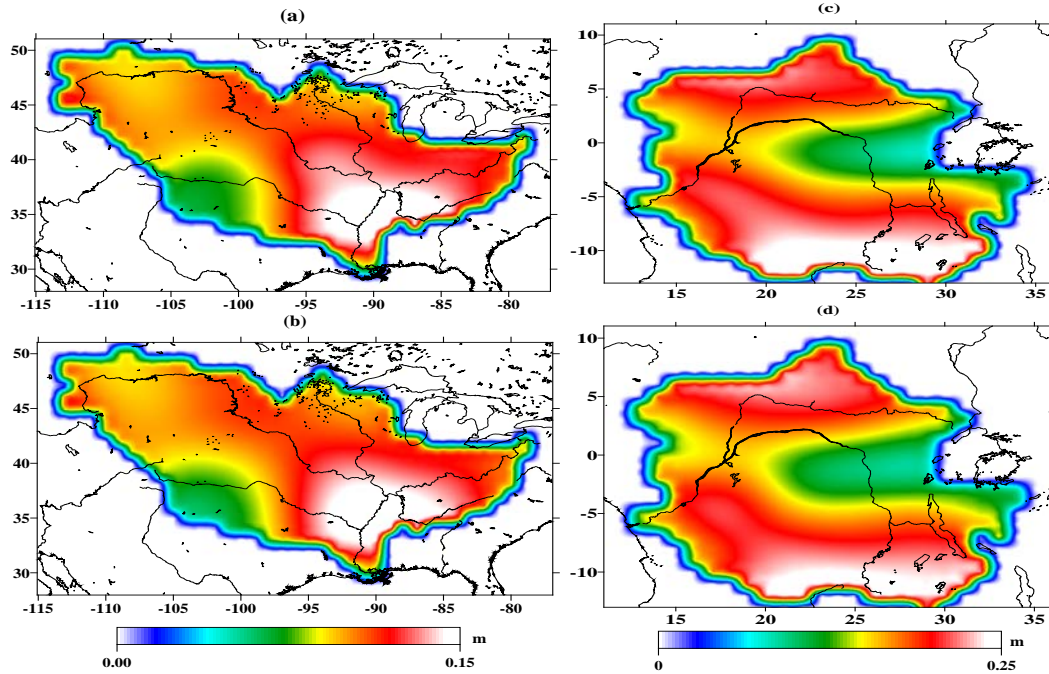


**Figure 13** Amplitudes of the mass changes of: (a) Mississippi River basin from CSR RL05; (b) Mississippi River basin from Tongji-GRACE02; (c) Congo River basin from CSR RL05; (d) Congo River basin from Tongji-GRACE02.

To investigate the noise level of the original and filtered GRACE solutions over these two basins, we present the RMS values of the residuals of these two River basins from the original and filtered GRACE solutions (i.e. CSR RL05 and Tongji-GRACE02) in Figures 14 and 15. We can find from Figures 14 and 15 that the RMS values of Tongji-GRACE02 are much less than those of CSR RL05 in the two basins for both original and filtered solutions. Especially for the case of the original solutions, the noise reductions of Tongji-GRACE02 are more pronounced compared to

those of CSR RL05. To support the above statements, the mean amplitudes and the mean RMS values of the residuals of the Congo and Mississippi River basins from the filtered and original solutions are given in Table 2. In spite of a little decrease of the amplitude occurs in Tongji-GRACE02 for the Congo River basin, the noise reductions of Tongji-GRACE02 solutions (especially the original solution) are much more pronounced than those of CSR RL05 in both two basins, suggesting that the larger signal to noise ratio is possessed by Tongji-GRACE02.

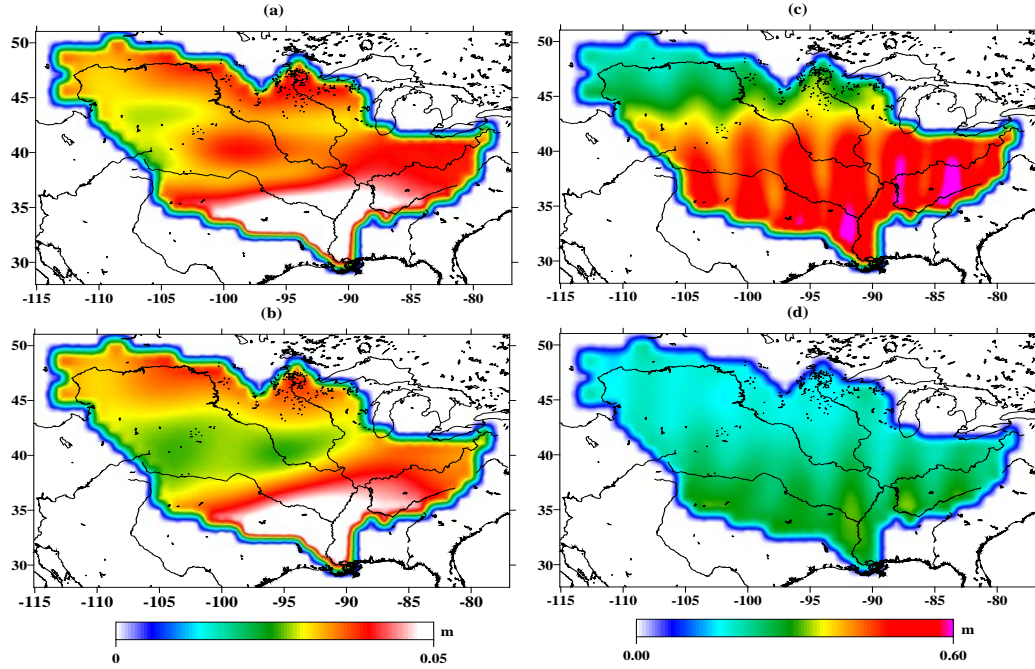


**Figure 14** RMS values of the residuals of the Mississippi River basin from: (a) filtered CSR RL05; (b) filtered Tongji-GRACE02; (c) original CSR RL05; (d) original Tongji-GRACE02.

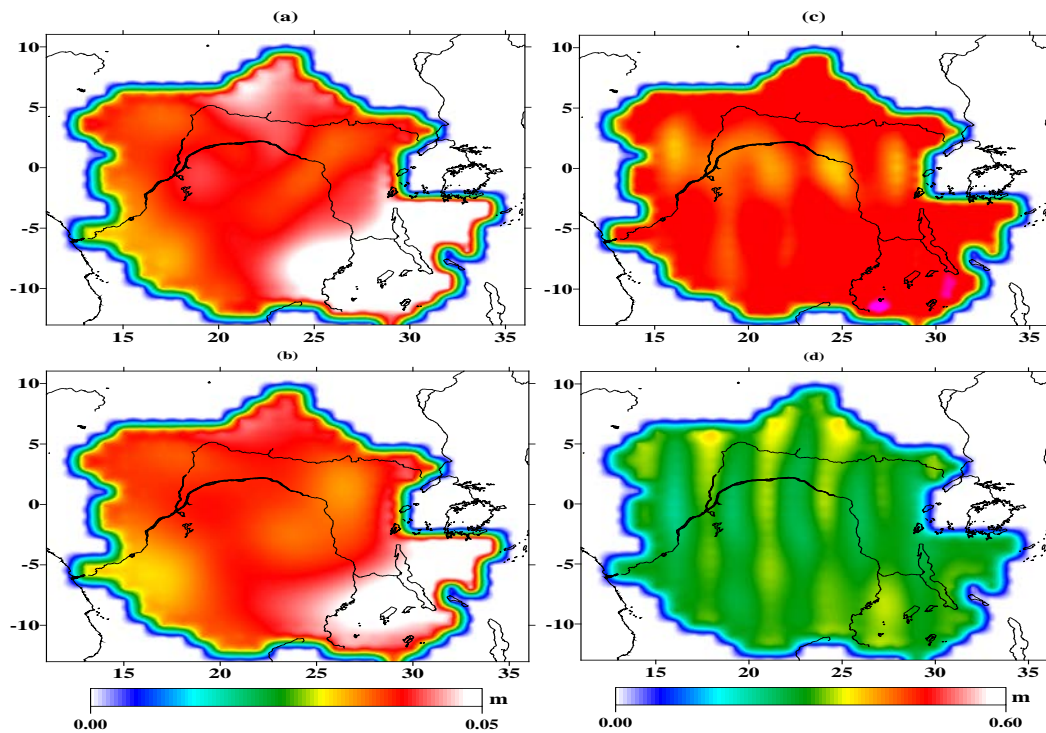


**Figure 15** RMS values of the residuals of the Congo River basin from: (a) filtered CSR RL05; (b) filtered Tongji-GRACE02; (c) original CSR RL05; (d) original Tongji-GRACE02.

**Table 2** The mean amplitudes and the mean RMS values of the residuals of the Congo and Mississippi River basins from the filtered and original solutions.

River basin	Model and Reduction	Amplitude	RMS of residuals of filtered solution	RMS of residuals of original solution
Mississippi	CSR RL05	10.9 cm	3.5 cm	40.6 cm
	Tongji-GRACE02	10.6 cm	3.2 cm	21.6 cm
	Reduction	3%	9%	88%
Congo	CSR RL05	17.6 cm	4.2 cm	48.6 cm
	Tongji-GRACE02	17.2 cm	3.9 cm	29.2 cm
	Reduction	2%	8%	66%

### 5.3 Mass variation tests in four desert areas

To develop more insights into the quality of these GRACE solutions, we compute the mass changes in the **Australia desert** of Jan. 2008 without employing any smoothing and decorrelation filtering. The resulting mass changes are shown in Figure 16, which reveals that Tongji-GRACE02 solution has the least mass change over the **Australian desert**, and GFZ RL05a has the second least mass change. The standard deviations of the mass changes for CSR RL05, GFZ RL05a, JPL RL05 and Tongji-GRACE02 are 48.32 cm, 37.45 cm, 58.25 cm and 19.64 cm, respectively. After applied with a 300 km Gaussian smoothing and a  $P_4M_6$  decorrelation filtering, the mass changes are presented in Figure 17, where the noise of these four GRACE solutions is significantly reduced by the smoothing and filtering and Tongji-GRACE02 solution still has the least mass change over the **Australian desert** among these GRACE solutions. The standard deviations are 2.38 cm, 2.41 cm, 2.20 cm and 1.63 cm for the filtered solutions of CSR RL05, GFZ RL05a, JPL RL05 and Tongji-GRACE02. Without using any smoothing and decorrelation filtering, we present the mass changes in the Australia, Kalahari, Karakum and Thar deserts over the period Jan. 2003 to Dec. 2012 by using these four GRACE solutions in Figure 18. As shown in Figure 18, Tongji-GRACE02 solution has the least mass change among the four solutions for all desert regions. After using the Gaussian smoothing with a 300 km radius and the  $P_4M_6$  decorrelation filtering, the four time series are displayed in Figure 19, where Tongji-GRACE02 solution agrees well with the other three solutions.



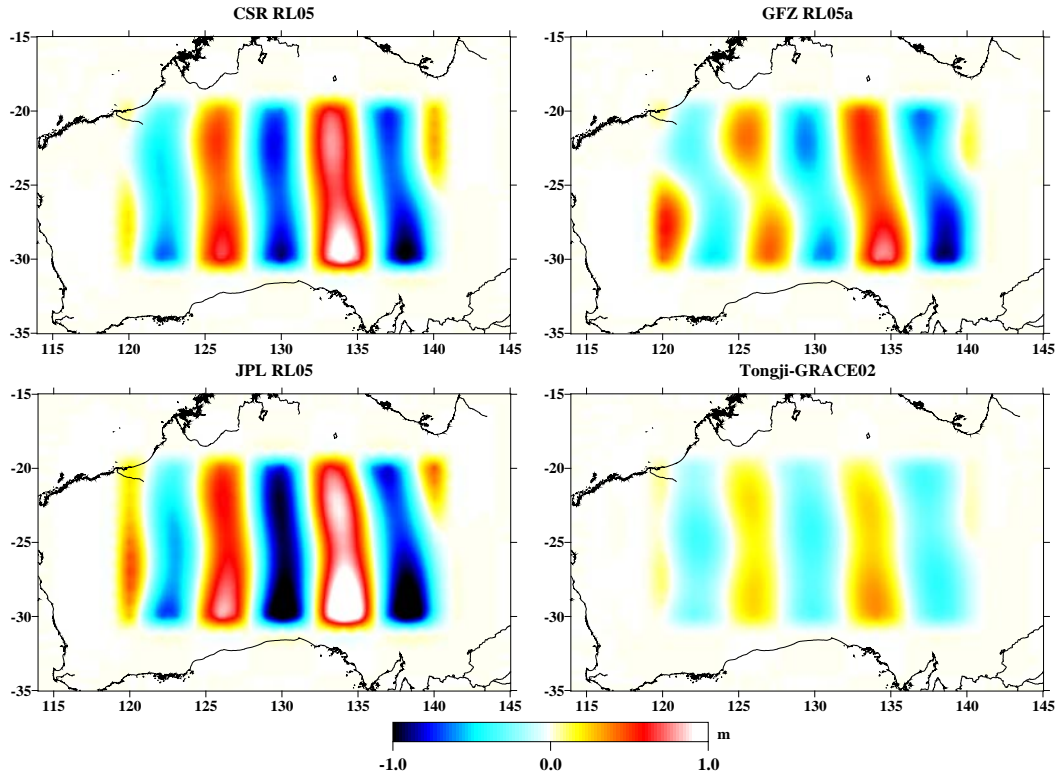


**Figure 16** Mass changes of Jan. 2008 (in EWH) inferred from CSR RL05, GFZ RL05a, JPL RL05, and Tongji-GRACE02 for the **Australian desert** without using any smoothing and decorrelation filtering.

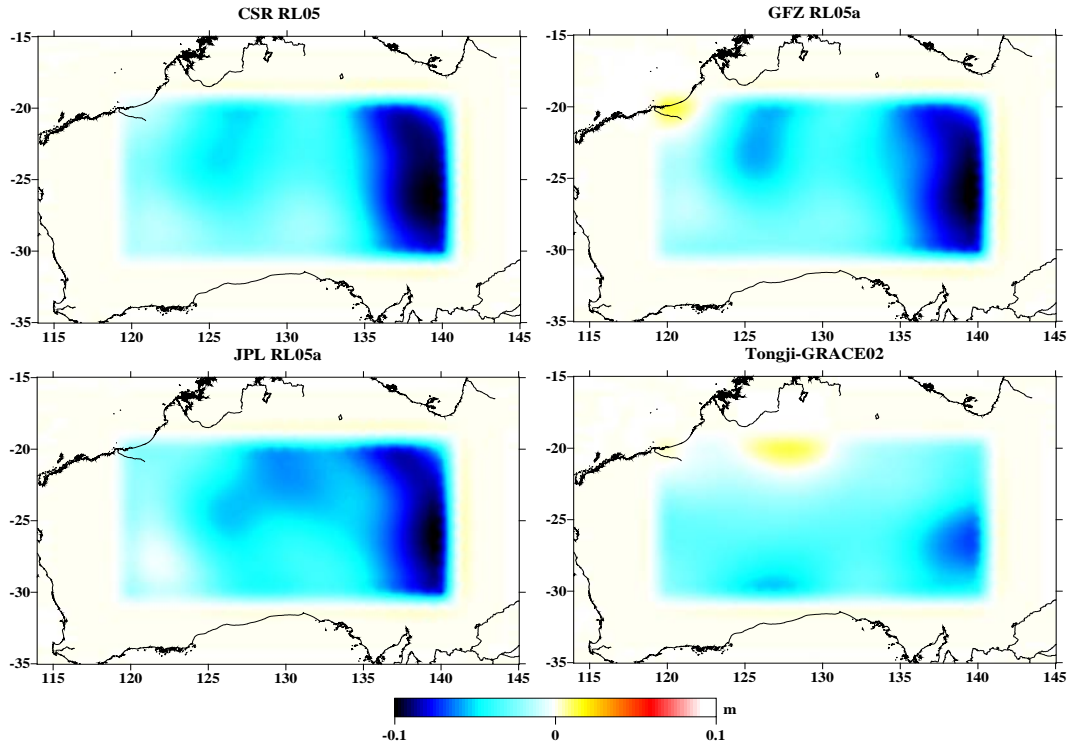


**Figure 17** Mass changes of Jan. 2008 (in EWH) inferred from CSR RL05, GFZ RL05a, JPL RL05, and Tongji-GRACE02 for the **Australian desert** using a 300 km Gaussian smoothing and a  $P_4M_6$  decorrelation filtering.

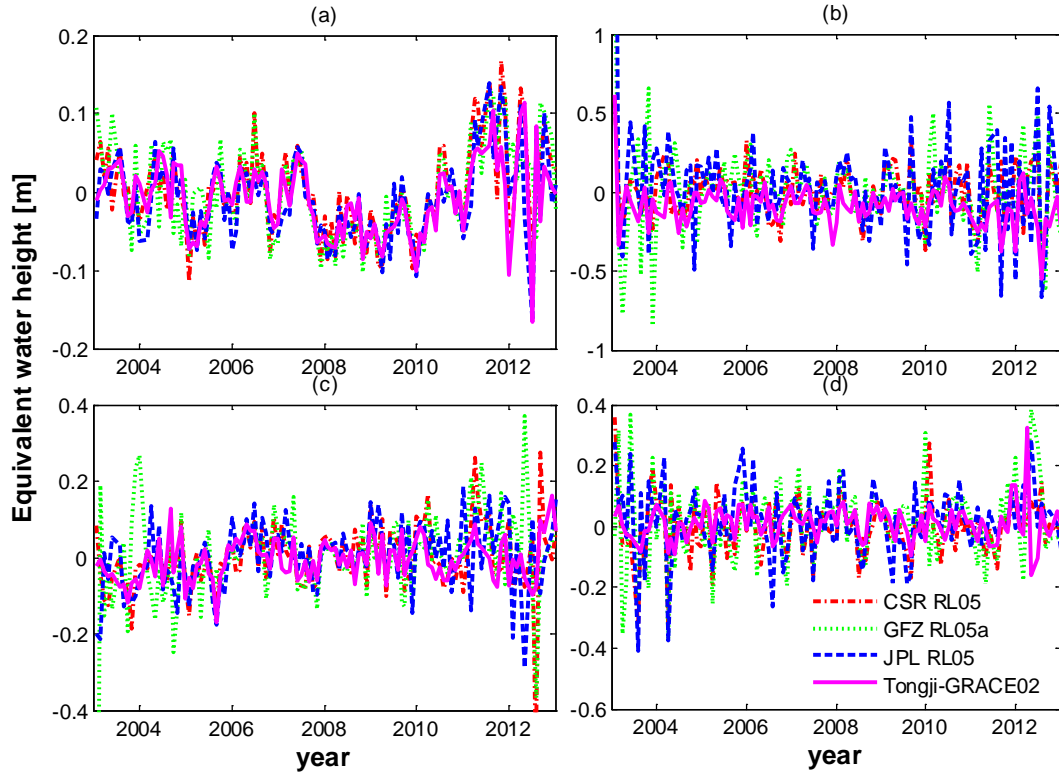


**Figure 18** Time series of mass changes (in EWH) inferred from CSR RL05, GFZ RL05a, JPL RL05, and Tongji-GRACE02 for the period Jan. 2003 to Dec. 2012 without applying any smoothing and decorrelation filtering:  
(a) Australia desert; (b) Karakum desert; (c) Kalahari desert; (d) Thar desert.

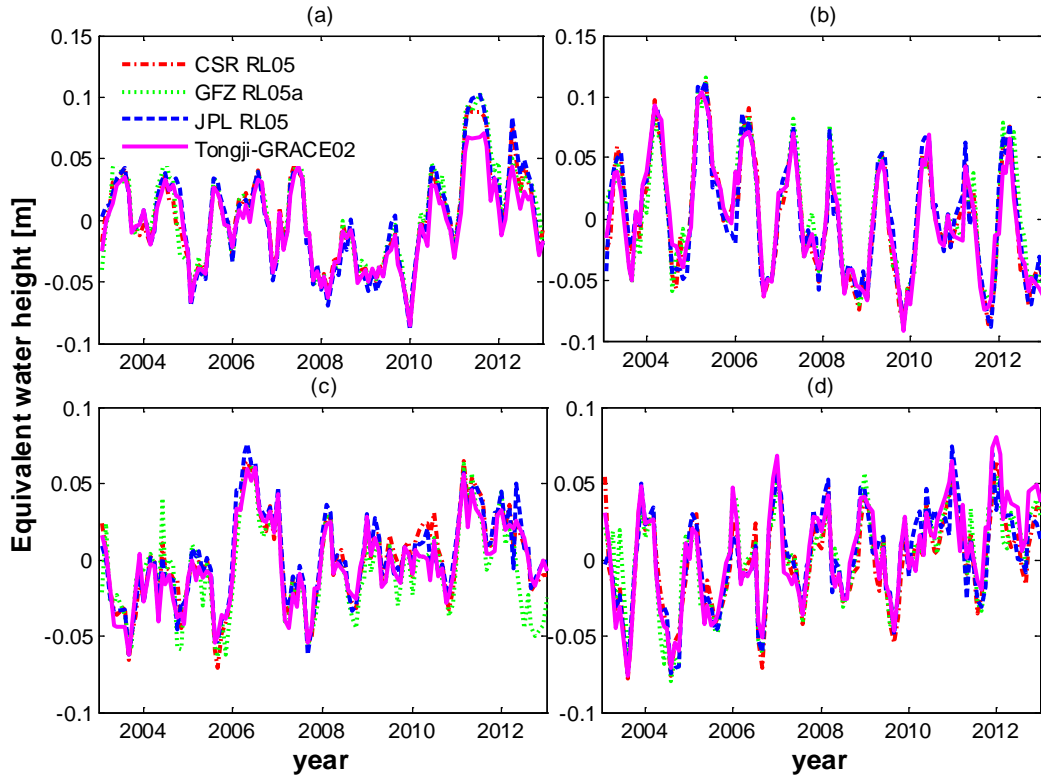


**Figure 19** Time series of mass changes (in EWH) from CSR RL05, GFZ RL05a, JPL RL05, and Tongji-GRACE02 for the period Jan. 2003 to Dec. 2012 after applying a 300 km Gaussian smoothing and a  $P_4M_6$  decorrelation filtering: (a) Australia desert; (b) Karakum desert; (c) Kalahari desert; (d) Thar desert.

For further assessment of the four GRACE solutions, we use the smoothing radiuses of 0 km, 180 km and 300 km to compute the mass change time series in the four deserts based on the four solutions. A small soothing radius is helpful to compare the noise of the GRACE solutions since a larger smoothing radius will lead to much more reductions of noise. After the bias, acceleration, annual, semiannual, trend, and the S2 alias terms are removed as Wahr et al (2006), the mean RMS values of the residuals in the four deserts from the four GRACE solutions are presented in Table 3. The  $P_4M_6$  decorrelation filtering is employed for all tests in Table 3 except for the case with the smoothing radius of 0 km. Table 3 reveals the following conclusions: (1) the noise of the GRACE solutions will be decreased to a large extent when increasing the smoothing radius; (2) Tongji-GRACE02 has the least RMS values of the mass changes in the desert tests among the four GRACE solutions no matter what kind of smoothing radius is applied; and (3) about 60% of improvements over deserts relative to CSR RL05 are achieved by Tongji-GRACE02 for the case of without using Gaussian smoothing and decorrelation filtering.

**Table 3** The mean RMS values of mass changes (unit is cm of EWH) over deserts from the four GRACE solutions after removing the bias, acceleration, annual, semiannual, trend, and the S2 alias terms.

Radius	Model and RMS reduction	Australia desert	Kalahari desert	Karakum desert	Thar desert
0 km	CSR RL05	46.17	46.89	33.85	45.18
	GFZ RL05a	52.71	57.83	54.92	61.25
	JPL RL05	58.32	46.67	53.11	52.96
	Tongji-GRACE02	28.68	27.78	21.21	26.09
	RMS reduction	61.0%	68.8%	59.6%	73.2%
180 km	CSR RL05	5.70	5.03	3.90	3.66
	GFZ RL05a	5.00	4.46	3.79	3.69
	JPL RL05	5.22	4.61	4.12	3.90
	Tongji-GRACE02	4.28	3.86	3.45	3.22
	RMS reduction	33.2%	30.3%	13.0%	13.7%
300 km	CSR RL05	3.54	3.01	3.02	2.21
	GFZ RL05a	3.48	3.16	2.89	2.23
	JPL RL05	3.54	3.06	3.07	2.39
	Tongji-GRACE02	3.10	2.82	2.81	2.12
	RMS reduction	14.2%	6.7%	7.5%	4.2%

## 6. Comparison with GLDAS model over St. Lawrence River basin

Hydrological processes is a leading cause of mass redistribution over land, which is usually computed by hydrological models such as GLDAS model and WGHM data (WaterGAP Global Hydrology Model, Famiglietti et al. 2011). Piretzidis et al. (2015) showed a good agreement between GRACE solution and GLDAS model, in which the RMS value of the difference of the time



series of the mass changes over St. Lawrence River basin for the period Jan. 2003 to Jun. 2014 computed from GRACE and GLDAS is about 2.7 cm. The GLDAS model, with  $1^\circ \times 1^\circ$  grid cell, was derived by the National Aeronautics and Space Administration (NASA) Goddard Space Flight Center (GSFC), and the National Oceanic and Atmospheric Administration (NOAA) National Centers for Environmental Prediction (NCEP). As recommend by Piretzidis et al. (2015), we use the GLDAS Noah model to compare the time series of the mass change over the St. Lawrence River basin for the period Jan. 2003 to Dec. 2012 to that from the four GRACE solutions, due to the lack of more accurate gravity measurements. To ensure a fair comparison between the GRACE solutions and GLDAS model, the GLDAS grid points are converted into spherical harmonic coefficients up to degree and order 60. Using a Gaussian smoothing of 300 km radius and a  $P_4M_6$  decorrelation filtering, five mass change time series in the St. Lawrence River basin derived from GLDAS, CSR RL05, GFZ RL05a, JPL RL05 and Tongji-GRACE02 are illustrated in Figure 20. It demonstrates that the seasonal changes in the St. Lawrence River basin can be picked up by both GRACE and GLDAS models, whereas a significant difference of amplitudes occurs between GRACE and GLDAS results, which is probably due to that GLDAS model does not include ground water variation. In an attempt to further evaluate the difference between GRACE and GLDAS, we compute the annual amplitudes and phases for all solutions, as well as the correlation coefficients and RMS values between GRACE solutions and GLDAS model. The results given in Table 4 suggest that Tongji-GRACE02 is closest to GLDAS model in terms of correlation coefficient, RMS value of mass change difference, and annual phase. Especially the annual phases from Tongji-GRACE02 and GLDAS are almost the same, with 28.0 degree for Tongji-GRACE02 and 30.1 degree for GLDAS. The RMS values of the differences of the mass changes between GLDAS model and CSR RL05, GFZ RL05a, and JPL RL05 as well as Tongji-GRACE02 are 3.9 cm, 3.9 m, 3.5 cm and 3.3 cm, which are close to the number in Piretzidis et al. (2015).

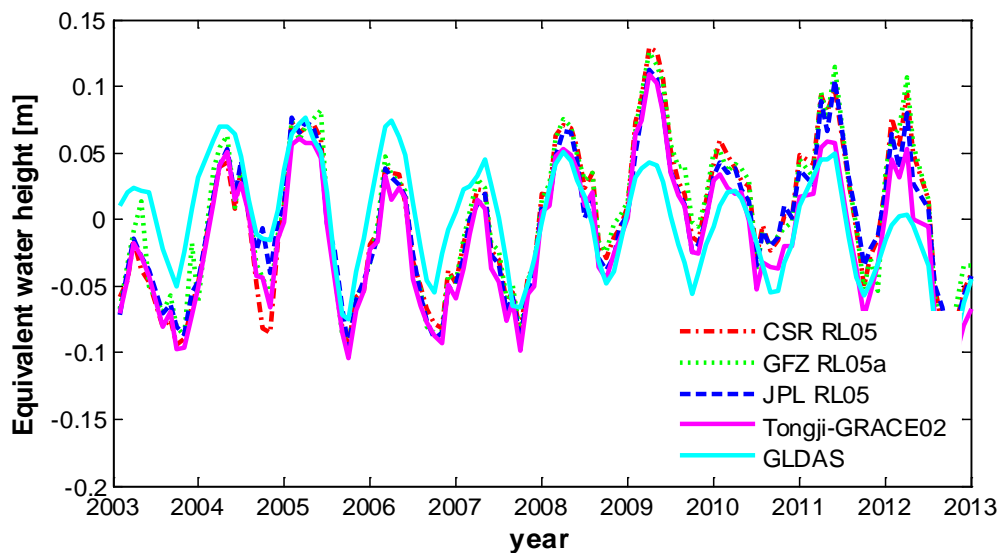


**Figure 19** Mass changes (in EWH) over the St. Lawrence River basin from GRACE solutions and the GLDAS model

**Table 4** The statistic results of the differences of mass changes (in EWH) over St. Lawrence River basin between the GRACE solutions and the GLDAS data.

Model	Correlation coefficient (%)	RMS (cm)	Annual amplitude (cm)	Annual phase (degree)
GLDAS	-	-	4.8	30.1
CSR RL05	68	3.9	5.8	38.0
GFZ RL05a	70	3.9	5.8	56.3
JPL RL05	71	3.5	5.3	68.7
Tongji-GRACE02	76	3.3	5.5	28.0

## 7. Conclusions

This paper presents an improved GRACE monthly gravity field solutions through modelling the errors of the non-conservative acceleration and attitude observations. The geopotential coefficients and the accelerometer biases are estimated using a weighted least squares adjustment, and the corrections of the orbit and range-rate measurements, as well as the attitude and non-conservative acceleration measurements are solved in the adjustment. Using the official GRACE data released by JPL, a new time series of GRACE monthly models over the period Jan. 2003 to Dec. 2012 has been derived.

The modelling of the non-conservative acceleration and attitude errors can effectively improve the gravity field solution, especially the modelling of the non-conservative acceleration errors is more important. The comparisons of mass changes over global ocean between Tongji-GRACE02 and the official GRACE solutions (i.e. CSR RL05, GFZ RL05a and JPL RL05) show that Tongji-GRACE02 solution has the least noise over the ocean, with about 21%, 74% and 42% of improvement relative to CSR RL05, GFZ RL05a and JPL RL05. For the test in the River basins (Mississippi and Congo) with strong seasonal signals, the mass changes of Tongji-GRACE02 solution agree well with those of the official GRACE solutions, with the correlation coefficients equal or larger than 0.98. Tongji-GRACE02 is also demonstrated to have the consistent mass changes with the official solutions in the continents selected (India, South America and Southeast Asia). Nevertheless, the analyses of signals and noise in both river basins and continents selected confirm that the signal to noise ratio of Tongji-GRACE02 is larger than that of CSR RL05. The comparisons of mass changes over the deserts between Tongji-GRACE02 and the official GRACE solutions reveal that Tongji-GRACE02 performs the best with the smallest mean RMS values. The mass changes in the St. Lawrence River basin derived from the GRACE solutions show a good agreement with those from the GLDAS data, where Tongji-GRACE02 solution also has the best agreement (especially in terms of the annual phase) with the GLDAS data.

## Acknowledgements

This work is mainly supported by National Natural Science Foundation of China (41474017) and National key Basic Research Program of China (973 Program; 2012CB957703). It is also partly sponsored by National Natural Science Foundation of China (41274035) and State Key Laboratory of Geodesy and Earth's Dynamics (SKLGED2014-1-3-E) and State Key Laboratory of Geo-information Engineering (SKLGIE2014-M-1-2). **Three reviewers and the associate editor, Prof. Kusche, as well as the editor in chief, Prof. Klees, are acknowledged for their constructive comments and suggestions.** We also thank JPL for providing us the GRACE level-1B data in this paper.

## References

- Bandikova T, Flury J, Ko UD (2012). Characteristics and accuracies of the GRACE inter-satellite pointing. *Adv. Space Res.*, 50(1), 123-135.
- Bandikova T, Flury, J (2014). Improvement of the GRACE star camera data based on the revision of the combination method. *Adv. Space Res.*, 54(9), 1818-1827.
- Bettadpur S (2009) Recommendation for a-priori Bias & Scale Parameters for Level-1B ACC Data (Version 2). URL: <http://podaac.jpl.nasa.gov/gravity/grace-documentation>.
- Bettadpur S (2012). Gravity Recovery and Climate Experiment UTCSR Level-2 Processing Standards Document for Level-2 Product Release 0005, Center for Space Research, Uni. of Texas, Austin.
- Beutler G, Jäggi A, Mervart L, Meyer U (2010). The celestial mechanics approach: application to data of the GRACE mission. *J. Geod.*, 84(11), 661-681.
- Bruinsma S, Lemoine J M, Gegout P, Biancale R, Bourgogne S (2014). Updated Release 3 of the GRACE Gravity Solutions from CNES/GRGS. In AGU Fall Meeting Abstracts (Vol. 1, p. 0410).
- Chen JL, Wilson CR, Famiglietti JS, Rodell M (2005). Spatial sensitivity of the Gravity Recovery and Climate Experiment (GRACE) time-variable gravity observations. *J. Geophys. Res.*, 110(B8), B08408.
- Chen JL, Wilson CR, Blankenship D, Tapley BD (2009a). Accelerated Antarctic ice loss from satellite gravity measurements. *Nat. Geosci.*, 2(12), 859-862.
- Chen JL, Wilson CR, Seo KW (2009b). S2 tide aliasing in GRACE time-variable gravity solutions. *J. Geod.*, 83(7), 679-687.
- Chen JL, Li J, Zhang Z, Ni S (2014). Long-term groundwater variations in Northwest India from satellite gravity measurements. *Global Planet. Change*, 116, 130-138.
- Chen Q, Shen Y, Zhang X, Hsu H, Chen W, Ju X, Lou L (2015a). Monthly gravity field models derived from GRACE Level 1B data using a modified short arc approach. *J. Geophys. Res.*, 120(3), 1804-1819.
- Chen Q, Shen Y, Zhang X, Hsu H, Chen W (2015b). Global Earth's gravity field solution with GRACE orbit and range measurements using modified short arc approach. *Acta Geod. Geophys.*, 50(2), 173-185.
- Chen Q, Shen Y, Zhang X, Hsu H, Chen W (2015c). Tongji-GRACE01: A GRACE-only Static Gravity Field Model Recovered From GRACE Level-1B Data using Modified Short Arc Approach. *Adv. Space Res.*, 56(5), 941-951.
- Chen Q, Shen Y, Chen W, Zhang X, Hsu H, Ju X (2015d). A Modified Acceleration-based Monthly Gravity Field Solution from GRACE Data. *Geophys. J. Int.*, 202(2), 1190-1206.
- Cheng M, Tapley BD (2004). Variations in the Earth's oblateness during the past 28 years. *J. Geophys. Res.*, 109(B9), B09402.
- Dahle C, Flechtner F, Gruber C, König D, König R, Michalak G, Neumayer KH (2012). GFZ GRACE Level-2 Processing Standards Document for Level-2 Product Release 0005. Scientific Technical Report-Data, p.12, doi: 10.2312/GFZ.b103-1202-25.
- Flury J, Bettadpur S, Tapley BD (2008). Precise accelerometry onboard the GRACE gravity field satellite mission. *Adv. Space Res.*, 42(8), 1414-1423.

- Famiglietti JS, Lo M, Ho, SL, Bethune J, Anderson KJ, Syed TH, Swenson SC, de Linage, CR, Rodell M (2011). Satellites measure recent rates of groundwater depletion in California's Central Valley. *Geophys. Res. Lett.*, 38(3), L03403.
- Frommknecht B (2007). Integrated sensor analysis of the GRACE mission (Doctoral dissertation), TU München.
- Horwath M, Lemoine JM, Biancale R, Bourgogne S (2011). Improved GRACE science results after adjustment of geometric biases in the Level-1B K-band ranging data. *J. Geod.*, 85(1), 23-38.
- Han SC, Shum CK, Jekeli C (2006). Precise estimation of in situ geopotential differences from GRACE low-low satellite-to-satellite tracking and accelerometer data. *J. Geophys. Res.*, 111(B4), B0441.
- Inácio P, Ditmar P, Klees R, Farahani HH (2015). Analysis of star camera errors in GRACE data and their impact on monthly gravity field models. *J. Geod.*, 89(6), 551-557.
- Jekeli C (1981). *Alternative methods to smooth the Earth's gravity field. Report 327. Department of Geodetic Science and Surveying, Ohio State University, Columbus.*
- Kang Z, Tapley B, Bettadpur S, Ries J, Nagel P, Pastor R (2006a). Precise orbit determination for the GRACE mission using only GPS data. *J. Geod.*, 80(6), 322-331.
- Kang Z, Tapley B, Bettadpur S, Ries J, Nagel P (2006b). Precise orbit determination for GRACE using accelerometer data. *Adv. Space Res.*, 38(9), 2131-2136.
- Klees R, Zapreeva EA, Winsemius HC, Savenije HHG (2007). The bias in GRACE estimates of continental water storage variations. *Hydrol Earth System Sci. Discussions*, 11(4), 1227-1241.
- Klinger B, Mayer-Gürr T. Combination of GRACE star camera and angular acceleration data: impact on monthly gravity field models. Oral presentation at the GRACE Science Team Meeting, Sept. 29, 2014, Potsdam.
- Kurtenbach E, Mayer Gürr T, Eicker A (2009). Deriving daily snapshots of the Earth's gravity field from GRACE L1B data using Kalman filtering. *Geophys. Res. Lett.*, 36(17), L1710.
- Kusche J, Schmidt R, Petrovic S, Rietbroek R (2009). Decorrelated GRACE time-variable gravity solutions by GFZ, and their validation using a hydrological model. *J. Geod.*, 83(10), 903-913.
- Liu X, Ditmar P, Siemes C, Slobbe DC, Revtova E, Klees R, Riva R, Zhao Q (2010). DEOS Mass Transport model (DMT-1) based on GRACE satellite data: methodology and validation. *Geophys. J. Int.*, 181(2), 769-788.
- Loomis BD, Luthcke SB (2014). Optimized signal denoising and adaptive estimation of seasonal timing and mass balance from simulated GRACE-like regional mass variations. *Adv. Adapt. Data Anal.*, 6(01), 1450003.
- Luthcke SB, Sabaka TJ, Loomis BD, Arendt AA, McCarthy JJ, Camp J (2013). Antarctica, Greenland and Gulf of Alaska land-ice evolution from an iterated GRACE global mascon solution. *J. Glac.*, 59(216), 613-631.
- Mayer-Gürr T (2006). *Gravitationsfeldbestimmung aus der Analyse kurzer Bahnbögen am Beispiel der Satellitenmissionen CHAMP und GRACE*, Dissertation, University of Bonn.
- Mayer-Gürr T, Eicker A, Ilk KH (2007). ITG-Grace02s: a GRACE gravity field derived from range measurements of short arcs. In gravity field of the Earth, proceedings of the 1st international symposium of the international gravity field service (IGFS), Istanbul. *Harita Dergisi* (Vol. 18, pp. 193-198).
- Mayer-Gürr T, Zehentner N, Klinger B, Kvas A. ITSG-Grace2014: a new GRACE gravity field release computed in Graz. Oral presentation at the GRACE Science Team Meeting, Sept. 29, 2014, Potsdam.
- Mayer-Gürr T, Kurtenbach E, Eicker A, Kusche J (2010). *ITG-Grace2010 gravity field model*. URL: [www.igg.uni-bonn.de/apmg/index.Php](http://www.igg.uni-bonn.de/apmg/index.Php).
- Meyer U, Jäggi A, Beutler G (2012). Monthly gravity field solutions based on GRACE observations generated with the Celestial Mechanics Approach. *Earth Planet. Sci. Lett.*, 345, 72-80.
- Petit G, Luzum B (2010), *IERS conventions (2010) (No. IERS-TN-36), Bureau International Des Poids et Mesures Sevres, France.*
- Piretzidis D, Tsalis I, Rangelova E, Sideris MG. Evaluation of land hydrology models using filtered GRACE satellite

- data in North America. Poster at the 26<sup>th</sup> General Assembly of the International Union of Geodesy and Geophysics, June 25, 2015, Prague.
- Rodell M, Houser PR, Jambor UEA, Gottschalck J, Mitchell K, Meng CJ, Arsenault K, Cosgrove B, Radakovich J, Bosilovich M, Entin JK, Walker JP, Lohmann D, Toll D (2004). The global land data assimilation system. *Bulletin of the American Meteorological Society*, 85(3), 381-394.
- Rowlands DD, Ray RD, Chinn DS, Lemoine FG (2002). Short-arc analysis of intersatellite tracking data in a mapping mission. *J. Geod.*, 76(6), 307-316.
- Schmidt R, Flechtner F, Meyer U, Reigber C, Barthelmes F, Förste C, Stubenvoll R, König R, Neumayer K, Zhu S (2006). Static and time-variable gravity from GRACE mission data. In *Observation of the Earth System from Space* (pp. 115-129). Springer Berlin Heidelberg.
- Schneider M (1968). A general method of orbit determination. Report 1279, Royal Aircraft Establishment, Hants, UK, 1-4
- Shen Y, Chen Q, Hsu H, Zhang X, Lou L (2013). A modified short arc approach for recovering gravity field model. Oral presentation at the GRACE Science team Meeting, Oct.23-26, 2013, Center of Space Research, Uni. of Texas.
- Swenson S, Chambers D, Wahr J (2008). Estimating geocenter variations from a combination of GRACE and ocean model output. *J. Geophys. Res.*, 113(B8), B08410.
- Swenson S, Wahr J (2006). Post-processing removal of correlated errors in GRACE data. *Geophys. Res. Lett.*, 33(8), L08402.
- Velicogna I, Wahr J (2013). Time variable observations of ice sheet mass balance: Precision and limitations of the GRACE satellite data. *Geophys. Res. Lett.*, 40(12), 3055-3063.
- Watkins MM, Yuan DN (2012), GRACE JPL Level-2 Processing Standards Document For Level-2 Product Release 05, GRACE 327-744 (v 5.0).
- Watkins MM, Wiese DN, Yuan DN, Boening C, Landerer FW (2015). Improved methods for observing Earth's time variable mass distribution with GRACE using spherical cap mascons. *J. Geophys. Res.*, 120(4), 2648-2671.
- Wahr J, Swenson S, Zlotnicki V, Velicogna I (2004). Time-variable gravity from GRACE: First results. *Geophys. Res. Lett.*, 31(11), L11501.
- Wahr J, Swenson S, Velicogna I (2006). Accuracy of GRACE mass estimates. *Geophysical Research Letters*, 33(6).
- Wu SC, Kruizinga G, Bertiger W (2006). Algorithm theoretical basis document for GRACE level-1B data processing V1. 2. Jet Propulsion Laboratory, California Institute of Technology.
- Stanton R (2000). Science & mission requirements document. Jet Propulsion Laboratory. JPL D-15928.
- Tapley BD, Bettadpur S, Ries JC, Thompson PF, Watkins MM (2004a). GRACE measurements of mass variability in the Earth system. *Science*, 305(5683), 503-505.
- Tapley BD, Bettadpur S, Watkins M, Reigber C (2004b). The gravity recovery and climate experiment: Mission overview and early results. *Geophys. Res. Lett.*, 31(9), L09607.